Energy Balances of Curing Concrete Bridge Decks

GARY S. WOJCIK AND DAVID R. FITZJARRALD

Atmospheric Sciences Research Center, University at Albany, State University of New York, Albany, New York

(Manuscript received 20 November 2000, in final form 21 April 2001)

ABSTRACT

Atmospheric conditions for several days after concrete is poured influence the exothermic, temperature-dependent, hydration reactions of concrete's cementitious (binding) components. Because excessively high concrete temperatures or lack of water eventually can lead to cracking, the initial days are critical to determining the concrete's long-term durability. Accurate model forecasts of concrete temperatures and moisture would help engineers to determine an optimal time to pour. Such forecasts require adequate environmental predictions. Existing models of curing concrete bridge decks employed by engineers lack realistic boundary conditions and so cannot handle many atmospheric conditions. Atmospheric energy exchange parameterizations typically are intended for use over areas much larger than bridges and so may not be useful as boundary conditions in curing-concrete models. To determine proper boundary conditions for the curing-concrete model discussed here, energy balances of four curing concrete bridge decks were estimated from observations made in the atmosphere as well as inside the concrete. Common meteorological techniques to estimate energy balance terms were used to bound the estimates. Most (70%–85%) of the concrete heat transfer occurred at the bridge's top. Sensible, latent, net radiative, and runoff water (sprayed on the top surface) heat fluxes, respectively, contributed 6%–24%, 15%–58%, 10%–34%, and 0%–73% of the top surface heat transfer. Bottom heat transfer was less than 30% of the top surface transfer. Laboratory calorimetry and the energy balance results agree to within 20% that the hydration reactions evolved about 190 kJ kg^{-1} by 24 h after mixing. This agreement validates the exchange coefficients proposed for the heat and moisture balances of these small areas both during periods when the concrete generated heat and later when the concrete was more passive in its environment.

1. Introduction

Ambient atmospheric conditions can adversely influence the thermal and moisture structure of freshly poured concrete. If concrete becomes too warm or temperature gradients too large during the first several days after the concrete is poured or if there is insufficient water in the concrete, the concrete may crack or may not develop its maximum potential strength, reducing its long-term durability (e.g., FitzGibbon 1976a,b; Gopalan and Haque 1987; Neville 1996). Such durability problems contributed to the need to replace an average of 12 concrete bridge decks at an average annual cost of $20 million in New York State from 1995 to 1999 (K. McCarty, 1999, personal communication).

To determine those atmospheric and concrete conditions under which the concrete should not be placed, we are developing a model of the curing of concrete bridge decks to predict the concrete's thermal and moisture states during the first several days after placement. Changing atmospheric and concrete conditions can alter the concrete's thermal and moisture states by changing the energy balances of the deck. Though understanding these energy balances of curing concrete is critical to the model development, we have found no studies that estimate them.

In this paper, the complete energy balances of four curing concrete bridge decks in New York State are estimated from field measurements of atmospheric and concrete environments. A challenge of this work is to determine fluxes from a small surface (largest horizontal dimension is < 50 m) in a heterogeneous landscape with methods that are better suited for horizontally homogeneous areas. Several conventional methods for determining energy budgets are used: radiation and eddy flux measurements; and bulk transfer, Bowen ratio, Penman–Monteith, and Priestley–Taylor methods. Each method has limitations when applied to the bridge environment (discussed in section 2c), but the ensemble of predictions is used to bound the likely values of the energy balance terms. The amount of heat generated by the curing concrete (see section 1a), determined from calorimetry experiments and from the field data [see sections 2b(2) and 3d], provides verification of the ensemble surface flux estimates and the utility of our approach. From these balances, proper boundary conditions for the model, including proper atmospheric exchange coefficients, are determined.

Corresponding author address: Gary S. Wojcik, Atmospheric Sciences Research Center, 251 Fuller Road, Albany, NY 12203.
E-mail: gary@asrc.cestm.albany.edu

© 2001 American Meteorological Society

Unauthenticated | Downloaded 02/24/21 06:32 PM UTC

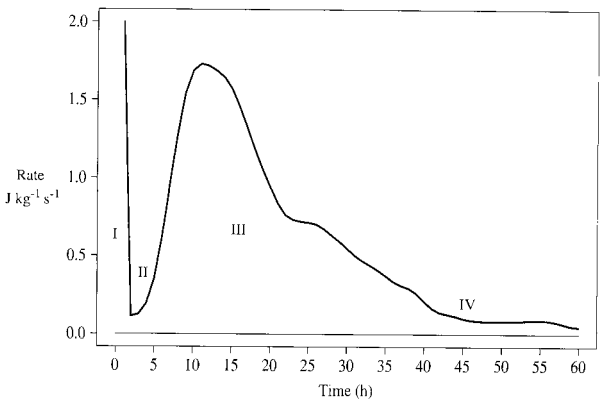

FIG. 1. A typical example of heat evolution rates (J kg^{-1} s^{-1}) for class-HP concrete, determined with a calorimetry experiment on a mixture of water with cement, flyash, and microsilica taken from the stock used at the 1999 bridge. For this calorimetry experiment, the temperature of the hydrating sample was kept at a constant temperature of 20°C. Roman numerals indicate the stages in the hydration process.

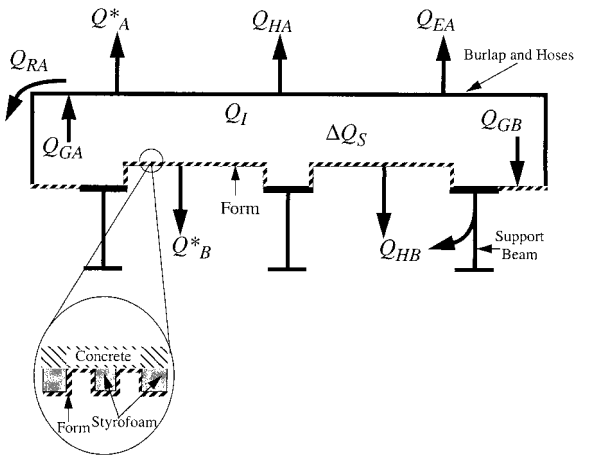

FIG. 2. A cross section of a curing concrete bridge deck with the energy balance terms. Subscripts A and B refer to those fluxes at the top and bottom of the bridge, respectively. Note that the bridges studied here have five or more support beams. The heavy arrows indicate the typical direction of energy transfer when the rapid heat evolution period (stage 3) occurs during the night.

a. Chemistry of curing concrete

Concrete is a mix of cementitious (binding) solids [e.g., cement (calcium silicates, calcium aluminates, and calcium aluminoferrites) and sometimes flyash (aluminates and silica) and microsilica], aggregate (sand and stones), and water. For its bridge decks, the New York State Department of Transportation (NYSDOT) now specifies the use of class-HP concrete whose cementitious component is composed of 74% cement, 20% flyash, and 6% microsilica by weight, a variation of class-H concrete, which uses 85% cement and 15% flyash. Concrete that contains flyash and microsilica is more durable and crack-resistant than concrete without these compounds (NYSDOT 1995).

The cementitious solids of concrete, upon mixing with water, react in highly exothermic, temperature-dependent hydration reactions (the higher the temperature, the faster the hydration reactions) producing a firm, hard mass. There are four major stages in the hydration reactions (Fig. 1): 1) surface reactions produce a ''gel'' on cementitious particles and release heat, lasting about 30 min, 2) hydration is slowed for several hours because diffusion of water into the cement particle is inhibited by the gel, 3) vigorous hydration and heat development occur for up to 20 h as water reaches unhydrated cement inside the gel coating (stiffening of the concrete occurs during this stage), and 4) hydration continues to decline for years. Stage 2 can be extended by the addition of retarders, which often have a chemical structure similar to sugar, into the concrete mix. The use of retarders is often necessary for large pours of concrete where the setting of one area before another could lead to cracking. By increasing the length of stage 2 with retarders, this problem can be avoided. The heat released from the hydration reactions is manifested in a rapid increase in concrete temperatures (up to 30°C in the case of a bridge deck) generally within the first 24 h after the concrete is poured.

b. Energy balances of a curing concrete bridge deck

Like most surfaces, bridge decks experience sensible, latent, radiative, and ground heat fluxes (Fig. 2). However, for a curing concrete deck, the energy balance also includes the hydration heat source and the bottom surface heat transfer from net radiation and sensible heat. In addition, excess water from irrigation hoses is sprayed on the top surface (covered with burlap) to facilitate the top surface reactions and to remove heat. These processes must be considered for inclusion in models and observed during field projects.

Previous modeling, field, and laboratory studies have been used by NYSDOT to develop specifications for conditions under which a pour is allowed. These empirical rules include that the air temperature must be 7°C or higher and the evaporation rate must be less than 830 W m^{-2} (NYSDOT 1999). These studies have limitations. For example, the laboratory and field studies, while suggesting that concrete cured at higher temperatures and lower humidities has decreased strength, have not involved realistic temporal variations of atmospheric variables (e.g., Hughes and Mahmood 1988; Tan and Gjorv 1996) or provide no specific guidelines about adverse atmospheric conditions under which a pour should not be allowed (e.g., Alsayed and Amjad 1994). In addition, although the evaporation rate is a placement specification and an important component of the energy balance, we have found no studies that have directly measured the evaporation rate from any concrete surface.

The most realistic modeling work in terms of boundary forcings was given by Plawsky and Kapila (1997)

Unauthenticated | Downloaded 02/24/21 06:32 PM UTC

TABLE 1. Information about the bridges studied in the field. Stage 2 and stage 3 refer to stages in the hydration process (see Fig. 1 and section 1a). For the ''Weather'' rows, T = air temperature, RH = relative humidity, and W = wind speed. The ''Average measurement height'' is the average distance above the bridges' top surfaces from which ''Weather'' measurements were taken.

Bridge	1995	1996	1998	1999
Dates	2–6 Aug	16–19 Sep	11–15 Jun	10–14 Jun
Location	Saratoga, NY	Rome, NY	Saratoga, NY	Amsterdam, NY
Length	25.6 m	45.7 m	46.3 m	27.4 m
Width	12.8 m	26.8 m	15.8 m	9.8 m
Thickness	0.29 m	0.29 m	0.29 m	0.29 m
Concrete volume	95 m^3	355 m^3	212 m^3	78 m^3
Average measurement height	2.9 m	2.4 m	2.7 m	0.9 m
Weather: Stage 2	2 Aug, day Partly cloudy W: 1.5 m s^{-1} T: 23°C RH: 75%	16–17 Sep, night Mostly cloudy/rain W: <1 m s^{-1} T: 15 °C RH: 90%	11 Jun, day Mostly cloudy W: 1.5 m s^{-1} T: 20°C RH: 70%	10 Jun, day Sunny W: 1.5 m s^{-1} T: 23°C RH: 55%
Weather: Stage 3	2–3 Aug, night Partly cloudy W: <0.5 m s^{-1} T: 18°C RH: 75%	17 Sep, day Mostly cloudy/rain W: <1 m s^{-1} T: 15°C RH: 90%	11–12 Jun, night Cloudy W: 1.2 m s^{-1} T: 16°C RH: 100%	10–11 Jun, night Clear W: <0.5 m s^{-1} T: 17°C RH: 85%
Concrete type	Class H	Class HP	Class HP	Class HP
Initial concrete temperature	29°C	25°C	23°C	23°C
Retarder [oz. (100 lb cementitious solids)$^{-1}$]	4	5.8	5	4

and Kapila et al. (1997) and included radiative, sensible, latent, and runoff water heat fluxes. They reported that the runoff water heat flux was an important heat removal mechanism, although no comparison with the other terms was given. Their heat exchange coefficients were derived from common engineering similarity expressions for flow over a flat, smooth plate. Since the bridge surface itself and the surrounding environment are typically rough surfaces, the smooth plate transfer coefficients may be too small. Also, a characteristic length chosen to compute the Reynolds number for use in the similarity expressions indicated laminar flow and unrealistically small coefficients over the bridge where turbulent conditions seem likely.

Other modeling studies have used poorly defined bulk heat exchange coefficients and a temperature difference between the concrete surface and the air as the boundary forcing, while neglecting evaporation, runoff water, and radiation heat transfer (e.g., Lachemi and Aïtcïn 1997; Ulm et al. 1998). Such parameterizations may not be realistic for atmospheric conditions other than those for which the model was validated. Because of these limitations, the utility of the current NYSDOT specifications is not known with any degree of certainty. There is a need for a modeling system that is flexible enough for use under any atmospheric conditions.

The development of our model begins here with a description of the energy balances of curing concrete bridges determined from our field observations. In section 2, a description of our four field campaigns including a description of our field setup and measurements and of our methodology for computing the energy balances is presented. Section 3 contains a discussion of the energy balances of the bridges, including our estimates of the amount of chemical heat produced by each concrete deck. A summary and discussion of the important findings and a discussion of our continuing work and potential applications of the present work are contained in section 4.

2. Methodology

a. Energy balances of a curing concrete bridge deck

The energy balances of three different regions of the bridge deck are considered: 1) top surface, 2) bottom surface, and 3) internal volume (Fig. 2). Note that the ''form'' is a thin, shiny, corrugated, galvanized steel sheet supporting the concrete from below and is in between the steel support ''I'' beams. The steel beams and half of the steel form are in direct contact with the concrete. The other half of the steel form is covered by styrofoam, separating concrete from steel, to reduce the amount of concrete that is used. The concrete thickness varies from 24 cm above the form to 30 cm above the beams.

By convention, upward fluxes are positive. For the top surface (A)

$$-Q_A^* + Q_{GA} = Q_{HA} + Q_{EA} + Q_{RA}, \qquad (1)$$

where Q_A^* is the net radiation, Q_{GA} is the concrete heat flux, Q_{HA} is the sensible heat flux, Q_{EA} is the latent heat flux, and Q_{RA} is the runoff water heat flux.

Unauthenticated | Downloaded 02/24/21 06:32 PM UTC

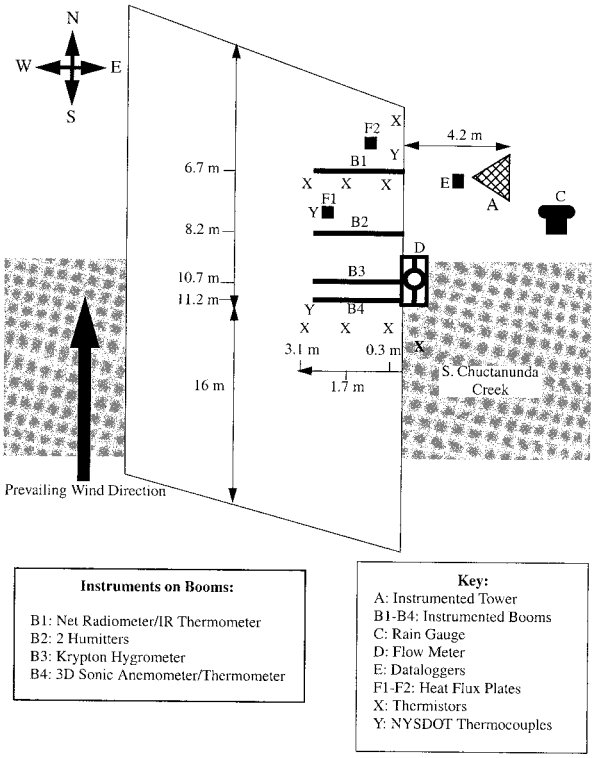

FIG. 3. Plan view (not to scale) of the locations of instruments and other hardware on the top and sides of the 1999 bridge. The large heavy arrow on the left side of the figure indicates the prevailing wind direction during this project. The arrow to the left of the "S. Chuctanunda Creek" label indicates the distances of thermistors (those south of B1 and B4, on the top of the concrete but below the burlap) from the east edge of the bridge. Note that the booms were attached to a vertical steel pole, anchored to the side of the bridge.

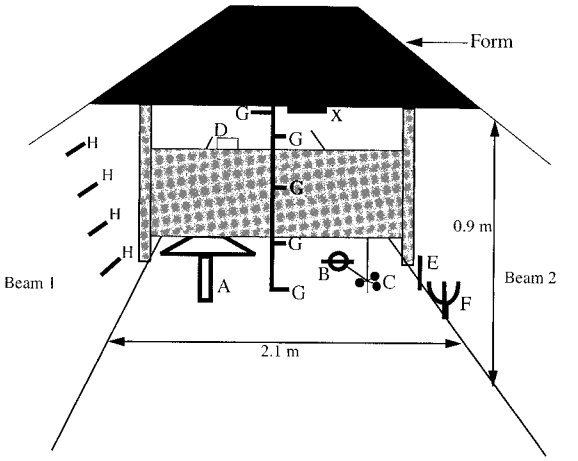

FIG. 4. Perspective view (not to scale) looking north to south (the direction of travel) of the area between two steel support beams where instruments were mounted during the 1999 bridge study. Note that thermocouples, G, measured air temperatures and were mounted vertically on a pipe between the beams. Thermocouples placed by NYSDOT, H, measured the beam temperatures and were taped to beam 1. Thermistor X was taped to the form.

At the bottom surface (B), there is no evaporation (no concrete is exposed at the bottom surface) or runoff water:

$$-Q_B^* + Q_{GB} = Q_{HB}, \tag{2}$$

where Q_{GB} is the concrete heat flux and Q_{HB} represents heat loss through the form and by conduction down the beams.

The internal volume balance equation is

$$\Delta Q_S = -Q_{GA} + Q_{GB} + Q_I, \tag{3}$$

where ΔQ_S is the storage term and Q_I is the hydration heat source.

By integrating over the entire volume of the bridge, Q_I is determined from the relation,

$$Q_I = Q_{HA} + Q_{EA} + Q_{RA} + Q_A^* - Q_{HB} - Q_B^* + \Delta Q_S, \quad \text{or} \tag{4}$$

$$Q_I = Q_{GA} - Q_{GB} + \Delta Q_S. \tag{5}$$

b. Field and laboratory measurements and predictions

1) FIELD MEASUREMENTS

The bridges studied are located in eastern and central New York State and have different horizontal dimensions (Table 1). Concrete for each bridge was placed during the summer months and experienced a variety of weather conditions while curing. Typically, our equipment was deployed a day or two before the concrete was poured and data were collected for the next 3 or 4 days. The data collection period covered the relatively dormant period (stage 2), the period of maximum heat evolution (stage 3), and the later periods when the concrete was generating a negligible amount of heat (stage 4) Stage 1 was already completed by the time the concrete trucks reached the bridges.

For the 1999 bridge, which had the most extensive bridge measurement campaign to date, instruments were placed on a tower, on booms directly over the deck, and on or near the top surface (Fig. 3 and Table 2). The booms were mounted to supporting pipes, anchored at the side of the bridge. To construct vertical gradients of temperature and humidity from the instruments above the bridge and on the tower, the raw data were corrected for any biases of a given instrument, as determined at our laboratory. Fast-response instruments were mounted

Unauthenticated | Downloaded 02/24/21 06:32 PM UTC

TABLE 2. Instruments deployed and variables measured near the 1999 bridge's top surface. See Fig. 3 for reference. NA = not applicable.

Variable	Instrument	Location	Height above deck
Air temperature and humidity	Campbell Scientific CS500 probes	Tower	2.5 m
Incoming shortwave radiation	Eppley Laboratories, Inc., PSP pyranometer	Tower	3 m
Wind speed	Met One Instruments, Inc., Model 014A cup anemometer	Tower	2 m
Wind speed and direction	Gill Instruments, Ltd., propeller vane anemometer	Tower	2.5 m
Net radiation	Campbell Scientific Q7 net radiometer	Boom 1	0.9 m
Deck skin temperature	Everest Interscience, Inc., Model 4021 infrared thermometer	Boom 1	0.08 m
Air temperature and humidity	Vaisala, Inc., Humitter 50Y probes	Boom 2	0.6 m and 1.4 m
High-frequency humidity	Campbell Scientific krypton KH20 hygrometer	Boom 3	0.9 m
High-frequency wind and temperature	Applied Technologies, Inc., 3-axis sonic anemometer and thermometer, Model SATI/3S	Boom 4	0.9 m
Deck surface/water temperatures	Campbell Scientific Model 108 thermistors	Surface/creek	0 m
Concrete heat flux	Radiation and Energy Balance Systems, Inc., Model HFT-3 soil heat flux plates	Concrete	3.5 cm below deck surface
Spray water volume	Seametrics, Inc., M-series flowmeter	Along side deck	NA
Precipitation	Campbell Scientific TE525 tipping bucket rain gauge	Nearby field	NA

on the booms to make direct eddy flux estimates of Q_{HA} and Q_{EA}. Below the bridge, instruments were mounted on and between support beams and on the form (Fig. 4 and Table 3).

Measurements were taken every second with Campbell Scientific, Inc., 23X dataloggers and the data were saved as 5-min averages, except for the fast-response measurements which were recorded at 1 Hz. Data were backed up periodically on Campbell Scientific CSM1 data storage cards and onto a PC.

The NYSDOT sampled temperatures every 30 min with copper–constantan thermocouples placed every 27 mm vertically within the concrete above the form and beams and vertically along the beams (Figs. 3 and 4). Infrared images of the top surface and a support beam were taken at the 1998 bridge with an Agema Infrared Systems, AB, Thermovision 870 thermal imaging system, which measures radiation between 2 and 5 μm. This instrument has a field of view of 20°. At a distance of 5 m from the specimen, the image width is 1.7 m.

TABLE 3. Instruments deployed and variables measured below the 1999 bridge's deck. See Fig. 4 for reference. NA = not applicable.

Variable	Instrument	Location	Distance below deck
Air temperature and humidity	Campbell Scientific CS500 probes	Beam bottom	0.9 m
Wind speed	C. W. Thornthwaite Associates Model WPRS106R cup anemometer	Beam bottom	0.9 m
Wind speed and direction	Handar, Inc., Model 425 2D ultrasonic anemometer	Beam bottom	0.9 m
Net radiation	Campbell Scientific Q7 net radiometer	Beam bottom	0.9 m
High-frequency vertical wind and temperature	Campbell Scientific CA27 sonic anemometer and fine wire thermocouple	Beam bottom	0.9 m
Form temperatures	Campbell Scientific Model 108 thermistors	Form	NA
Beam temperatures	Copper–constantan thermocouples	Beam	0.04–0.9 m
Air temperatures between beams	Copper–constantan thermocouples	Between beams	0.07–0.9 m
Form temperatures	Everest Interscience Model 4201 infrared thermometer	Between beams	0.2 m

Unauthenticated | Downloaded 02/24/21 06:32 PM UTC

With 140 × 140 pixels per image, the spatial resolution of each pixel at these distances is 1.2 cm.

The fast-response instruments were deployed only at the 1999 bridge, and the spray water was metered only at the 1998 and 1999 bridges. At the 1996 bridge, spray water volume was estimated by sampling the volume coming from many of the hose holes. No field estimates of spray water flow rate were made for the 1995 bridge. For the 1995 and 1996 bridges, no beam temperature data were collected, and for the 1995 bridge, the concrete temperatures recorded were those above the form, not above a beam.

2) Laboratory measurements

To provide an independent estimate of Q_I, calorimetry experiments were performed with samples of cement, flyash, and microsilica from the stock used for the 1998 and 1999 bridges. For the 1996 and 1995 bridges, the 1999 samples were used to provide an estimate. The starting temperatures of the mixtures placed in the calorimeter corresponded to the concrete temperatures at the time of placement at each bridge. The proper amount of cementitious components, water, and retarder was used (Table 1). The calorimetry setup consisted of a reaction chamber (~535 ml) created out of 3-in.-diameter copper tubing and end caps placed inside a water-filled 2-L Dewar flask, all enclosed in a R11 foamboard box packed with R38 fiberglass insulation. Thermocouples measured the cementitious mixture, surrounding water, and insulation temperatures as the sample hydrated for at least 72 h. Each sample's heat generation rate was determined from the cementitious mixture and water temperature changes and by estimating the heat loss from and the heat capacity of the calorimeter [see Wojcik et al. (2001), manuscript submitted to *Cem. Concr. Res.*, for more details on the calorimetry experiments].

To determine Q_{RA}, the temperatures of water drops from hoses as they hit the top surface must be known [see section 2c(3)]. These temperatures were estimated with a model by Pruppacher and Klett (1997) which requires the drop size data. The water drop sizes from hoses similar to those used at the bridge were measured with a ground-based precipitation probe, model GBPP-1000, from Particle Measuring Systems, Inc.

3) One-dimensional model

A 1D (vertical) finite difference model of the concrete deck, which uses the Crank–Nicolson scheme to solve the heat diffusion equation (Wojcik 2001), was used to determine the concrete thermal conductivity, which is needed to estimate Q_{GA}. The model boundary conditions include net radiation, runoff water, and latent and sensible heat fluxes.

c. Estimating the energy balances

1) Estimating sensible and latent heat fluxes (Q_{HA} and Q_{EA})

Q_{EA} and Q_{HA} were estimated with flux-gradient expressions and direct eddy flux measurements. The flux-gradient schemes, such as the Bowen ratio (BR), Penman–Monteith (PM), Priestley–Taylor (PT), and bulk transfer (BT) approaches, relate the vertical flux of a variable to its vertical gradient (Oke 1987; Garratt 1992). The BR, PM, and PT then use surface energy balances and other approximations to arrive at their final formulation. Note that for the flux-gradient relations, we assumed that the top surface of the bridge, which was covered by burlap and sprayed continuously with water, was saturated. While not under water at all locations, the burlap acted as a wick to absorb water much like the wick of a wet-bulb thermometer. The burlap also slowed the movement of water, resulting in tiny, visible pools of water in the pore spaces of the burlap. We therefore feel that our assumption that the surface was saturated is reasonable.

Implicit in the derivations of the universal forms of BR, PT, and PM is that the underlying surface must be horizontally homogeneous so that the flow and gradients are in equilibrium with the surface. In such a situation, our tower and surface measurements would give adequate estimates of the needed gradients. However, the top surfaces of the bridges studied only add to the heterogeneity of their landscape, which includes roads, forests, fields, construction equipment, houses, and rivers. The gradients computed with tower measurements may or may not be representative of the actual surface fluxes.

Because the curing bridge deck represents changes in surface roughness (rough to smooth), temperature, and moisture, an internal boundary layer (IBL) developed over each bridge. The IBLs may have had vertical gradients distinct from those obtained with the tower measurements. Therefore, the top surface fluxes may have been different from those indicated with the tower measurement gradients. To sample features of the expected IBL, temperature and humidity sensors and the fast-response instruments were placed directly over the 1999 bridge on booms.

(i) Penman–Monteith scheme

The Penman–Monteith combination parameterization (Penman 1948; Monteith 1965) includes an energy balance approach with an aerodynamic term that accounts for the evaporative power of air. We modify the original parameterization to include Q_{RA} in the total available energy (W m^{-2}):

$$Q_{EA} = \delta(-Q_A^* + Q_{GA} - Q_{RA}) + (1 - \delta)[\rho L_v C_e U(q_a^* - q_a)], \quad \text{and} \quad (6)$$

Unauthenticated | Downloaded 02/24/21 06:32 PM UTC

$$Q_{HA} = (1 - \delta)\{(-Q_A^* + Q_{GA} - Q_{RA}) - [\rho L_v C_h U(q_a^* - q_a)]\}. \quad (7)$$

See the appendix for definitions of variables.

(ii) Priestley–Taylor scheme

Priestley and Taylor (1972) found an empirical relation between latent heat flux and the total available energy given by $-Q_A^* + Q_{GA}$ for a saturated surface under advection-free conditions. We modify their original formulation for the bridge system by including Q_{RA} in the total available energy. The equations for Q_{EA} and Q_{HA} (W m^{-2}) become:

$$Q_{EA} = \alpha \frac{s}{(s + \gamma)}(-Q_A^* + Q_{GA} - Q_{RA}), \quad \text{and} \quad (8)$$

$$Q_{HA} = \frac{[(1 - \alpha)s + \gamma]}{(s + \gamma)}(-Q_A^* + Q_{GA} - Q_{RA}). \quad (9)$$

See the appendix for definitions of variables. The Priestley–Taylor parameter, α, is equal to 1.26 for water surfaces, including small lakes, and wet land surfaces under advection-free conditions (e.g., Stewart and Rouse 1977). It does, however, exhibit a seasonal variation from 1.2 in summer months to 1.5 during the winter and may be larger for smaller surfaces where advection is important (de Bruin and Keijman 1979).

(iii) Bowen ratio scheme

The Bowen ratio β may be written as

$$\beta = \frac{Q_{HA}}{Q_{EA}} = \frac{c_p(T_a - T_s)}{L_v(q_a - q_s)}, \quad (10)$$

where the exchange coefficients of heat and moisture are assumed to be equal. With β and the top surface energy balance given in Eq. (1), Q_{EA} and Q_{HA} (W m^{-2}) are given by

$$Q_{EA} = \frac{(-Q_A^* + Q_{GA} - Q_{RA})}{(1 + \beta)}, \quad \text{and} \quad (11)$$

$$Q_{HA} = \frac{\beta(-Q_A^* + Q_{GA} - Q_{RA})}{(1 + \beta)}. \quad (12)$$

(iv) Eddy fluxes, the IBL, and flux footprints

The depth and structure of the IBL depend on the upwind flow structure, the bridge's roughness, and the heat and mass fluxes to or from the bridge. The newly formed IBL will influence the surface fluxes and so must be investigated in relation to the energy balances of a curing bridge. The instruments on the booms above the 1999 bridge sampled the IBL.

Itier et al. (1994) suggested that a dry-to-wet transition can be treated as a step change in concentration, after which the difference between the downwind and upwind surface fluxes exhibits a $-1/6$ power-law dependence on the distance. However, Dyer and Crawford (1965) found that while the latent heat flux at a height of 4 m increased by up to 40% and nearly matched the surface value at a fetch of 200 m, the surface value changed only slightly.

Walmsey (1989) reviewed various methods to estimate IBL depth under neutral conditions and found the parameterization of Panofsky and Dutton (1984) to be the most reliable. They used u_* and σ_w to determine the growth rate. For an ideal fetch (wind blowing along the length of the bridge) and neutral conditions, at $X =$ 16 m (the midway point of the 1999 bridge) from the leading edge (Fig. 3), the IBL depth would be 1.3 and 1.8 m for roughness lengths of 0.002 and 0.01 m, respectively. With a heated surface, the growth rate may be proportional to $X^{1.4}$ (Rao 1975) suggesting more rapid IBL growth. Andreas and Cash (1999), based on observations over convective Arctic leads and polynyas, suggest an IBL depth at $X = 16$ m of 2.3 m. Their relation was developed from data that featured stronger winds and more intense thermal convection than experienced at the bridges.

With our sonic anemometer/thermometer and krypton hygrometer mounted directly above the 1999 bridge, Q_{HA} and Q_{EA} (W m^{-2}) were estimated as follows:

$$Q_{HA} = \rho c_{pd}(\overline{w'T'} + 0.84\overline{T}\,\overline{w'q'}), \quad \text{and} \quad (13)$$

$$Q_{EA} = \rho L_v \overline{w'q'}. \quad (14)$$

See the appendix for definitions of variables. The second term on the right-hand side of Eq. (13) accounts for the variation of the specific heat capacity of air with humidity (Brook 1978). The sonic anemometer measures T_v and so gives $\overline{w'T_v'}$ instead of $\overline{w'T'}$, which is generally lower than $\overline{w'T_v'}$ by 15% or less. The raw covariances were corrected to give the desired $\overline{w'T'}$.

Because the air parcels sampled by the flux instruments were affected by both the bridge and the upwind area, a footprint analysis was performed [see section 3b(1)ii]. The analytical footprint expressions given by Horst and Weil (1994) were developed with dispersion models for passive, conserved scalars and were based on the assumption that the turbulent flow field was horizontally homogeneous. According to this model, the flux footprint depends only on the separation between the measurement point and the surface source region, stability, and measurement height.

The turbulence above the bridges was most likely different than that upwind because of changes in surface convective fluxes and roughness. Such situations are not well understood in relation to footprint analysis and require further study. However, we feel the footprint expressions can lend insight into the fetch requirements needed to estimate the bridges' top surface fluxes with the direct eddy and other sensors.

Unauthenticated | Downloaded 02/24/21 06:32 PM UTC

We note that all air measurements, not just the direct eddy flux measurements, have a source area footprint. For scalar point measurements, the source areas are an order of magnitude larger than the corresponding direct eddy flux source areas (Schmid 1997). However, for scalar vertical profiles, the footprint is identical to or closer to the measurement location than that for the direct eddy flux (Horst 1997; Stannard 1997). In our analysis, we estimated vertical fluxes based on gradients determined from a surface value and an air value. Therefore, our flux estimates are not as limited by the source area problem as would be the case if we had used two air values.

(υ) Bulk transfer relations and exchange coefficients

By equating the estimated and measured fluxes with the BT relations, exchange coefficients were determined. In the BT approach, Q_{EA} and Q_{HA} (W m^{-2}), are given by

$$Q_{EA} = -\rho L_v C_e U(q_a - q_s), \quad \text{and} \tag{15}$$

$$Q_{HA} = -\rho c_p C_h U(T_a - T_s). \tag{16}$$

See the appendix for definitions of variables. It is often assumed that $C_h = C_e$ (e.g., Garratt 1992).

The estimates of $C_h = C_e = C$ were compared with free convection exchange speeds and drag coefficients, C_d. Kondo and Ishida (1997) determined exchange speeds [which take the place of C_eU and C_hU in Eqs. (15) and (16)] for free convection conditions ($z/L < -1$ or Rb < -1 and $U < 1$ m s^{-1}) over smooth or rough surfaces. They found that $CU = b(T_{sv} - T_{av})^{1/3}$, where b is 0.0011 for smooth surfaces and 0.0038 for rough surfaces. Kondo and Ishida's formulation, with the 1/3 dependence on T_{sv} and T_{av}, is consistent with the free convection scaling extension of Monin–Obukhov similarity hypothesis (MOSH) suggested by Wyngaard et al. (1971).

Drag coefficient C_d is given by

$$C_d = \left(\frac{u_*}{U}\right)^2. \tag{17}$$

For the 1999 bridge, u_* was determined directly from the fast-response instruments as $u_* = (\overline{u'w'_2} + \overline{v'w'_2})^{1/4}$. Here C_d and C are not identical. For example, under neutral conditions, with $z_0 = 0.006$ m and $z/z_0 = 150$, $C_d = 0.0064$ is approximately 30% greater than $C = 0.0045$. Under convective conditions and similar surface roughness, both C_d and C may be up to 1.75 times these values (Garratt 1992).

2) ESTIMATING THE CONCRETE HEAT FLUX (Q_{GA})

Here Q_{GA} was estimated in three ways. First, a value for concrete thermal conductivity, k_c, and the concrete temperature gradient near the top surface was used (discussed in more detail later in this section). Second, the other terms in Eq. (5) were estimated and Q_{GA} was determined by residual. Last, the data from the heat flux plates were used.

With k_c and the NYSDOT concrete temperature data, Q_{GA} (W m^{-2}) was computed directly as follows:

$$Q_{GA} = -k_c\frac{dT}{dz} - \rho_c c_{pc}\Delta z\frac{dT}{dt}. \tag{18}$$

See the appendix for definitions of variables. In practice, because the temperature gradients over the form may be different than those over the beams, an area-weighted average temperature gradient that considers both locations was used. For the 1999, 1998, and 1995 bridges, the area over the form is 80% and the area over the beams is 20% of the total bridge surface area (Fig. 2). These percentages are 70% and 30%, respectively, for the 1996 bridge.

The NYSDOT thermocouples within the concrete were anchored vertically every 27 mm. Over the beams, the concrete thickness is roughly 297 mm and over the form it is 243 mm. The NYSDOT thermocouple that measured the top surface temperature (between the burlap and concrete) was placed after the concrete was poured and smoothed. The amount of concrete that was actually poured determined the exact thickness of the top layer. The exact thickness of the top concrete layer is known within 50% or is between 14 and 41 mm, while the thickness of lower layers is known within 10%. To reduce the impact of the larger uncertainty of the top layer thickness on the computation of Q_{GA}, dT/dz was computed for the layer below the top layer of concrete and a storage term was computed [Eq. (18)]. The storage term accounts for between 10%–20% of the total Q_{GA} during most times in the 1999 field campaign. However, the storage term was the dominant portion of Q_{GA} (accounting for ± 100 W m^{-2}) near sunrise and sunset when energy was rapidly gained and lost by the top layer of concrete.

Scanlon and McDonald (1994) suggested that k_c varies from 2 to 4 W m^{-1} K^{-1} depending on the materials used. Two methods were used to estimate k_c from our field data to narrow the range of possibilities. First, Q_{GA} measured by the heat flux plates was divided by the linear concrete temperature gradient measured by NYSDOT thermocouples just above and just below the plate, over a distance of 27 mm. Second, the 1D finite-difference model was used. Because the predicted temperature gradients were much more sensitive to k_c than to the surface fluxes, k_c was estimated by adjusting its value in the model until the top-to-bottom concrete temperature difference matched the observed difference.

3) ESTIMATING THE RUNOFF WATER HEAT FLUX (Q_{RA})

Heat flux Q_{RA} (W m^{-2}) was computed by

$$Q_{RA} = -\rho_w c_w(T_{wi} - T_{wf})M/A. \tag{19}$$

Unauthenticated | Downloaded 02/24/21 06:32 PM UTC

See the appendix for definitions of variables. The runoff water flow rate was the total water incident on the bridge (from hoses and precipitation), less the amount needed to give Q_{EA}. Attempts were made to measure the runoff water flow rate with rain gutters and collection vessels, but because the water ran off in places where adequate sampling of the flow was not possible, the attempts were unsuccessful. The amount of water that evaporated was no more than 10% of the amount sprayed onto the bridge (see section 3c).

Variable T_{wf} was measured, and to compute Q_{RA}, T_{wi} had to be determined. A falling drop will experience heat and mass transfer with the air from conduction and evaporation, and this transfer is dependent on the drop size (Kinzer and Gunn 1951; Andreas 1995; Pruppacher and Klett 1997). The water drop sizes from irrigation hoses similar to those used at the bridge were measured with a ground-based precipitation probe. The drop sizes were well-represented by the Marshall–Palmer distribution (e.g., Rogers and Yau 1989) with a rainfall rate of 7 mm h^{-1}. About 90% of the falling drop water volume was from drops larger than 0.8 mm in diameter, and about 60% was from drops larger than 1.5 mm in diameter.

A 1-mm-diameter falling drop will need about 5 s to come within $1/e$ of its equilibrium temperature. The equilibrium temperature that the drops could reach is within about 0.5°C of the wet-bulb temperature of the air (Andreas 1990). Based on the measured drop size distribution, we estimate that the drops from the hoses remained in the air between 1 and 2 s and so did not have enough time to approach their equilibrium temperature. Therefore, a model given by Pruppacher and Klett (1997, p. 544) was used to determine T_{wi}. The model inputs include drop size, water temperature in the hoses, and air temperature and humidity. The model predictions of the time it takes a falling drop's temperature to come within $1/e$ of the equilibrium temperature are within 10% of an observed value given by Kinzer and Gunn (1951). The average water temperature of a given drop size range was estimated with the model. Variable T_{wi} was determined by weighting the drop temperature of each size range by its fractional contribution to the total rainfall rate from the hoses.

4) ESTIMATING HEAT TRANSFER AT THE BRIDGE BOTTOM (Q_{HB}, Q_{GB}, AND Q_B^*)

At the bridge bottom, heat transfer occurs by conduction along the steel support beams, conduction through the form and then aerodynamically from the form, and by net radiation. Variable Q_B^* was measured and Q_{GB} was determined by difference. Variable Q_{HB} was given by the sum of heat transferred through the form and the beams:

$$Q_{HB} = -\left(\frac{F_f \Delta T_{cf}}{\frac{\Delta Z_{cf}}{k_c} + \frac{\Delta Z_f}{k_f}}\right)_{FORM} - \left(\frac{F_s \Delta T_{cs}}{\frac{\Delta Z_{cs}}{k_c} + \frac{\Delta Z_s}{k_s}}\right)_{BEAMS}, \quad (20)$$

where the terms on the right hand side of Eq. (20) account for, respectively, loss through the form and down the beams by conduction through the concrete/steel interface. Because air temperatures between the beams indicate a very stable environment [see section 3b(6)], there is no appreciable aerodynamic heat loss from the form.

For the 1999 bridge, a fast-response sonic anemometer–thermometer was mounted to the bottom of a support beam. While not a direct measure of Q_{HB}, these measurements provided an estimate of heat being transferred between the beams, which is not expected to be radically different from Q_{HB}.

5) ESTIMATING THE CHEMICAL HEAT SOURCE AND STORAGE (Q_I AND ΔQ_S)

The amount of hydration heat generated was estimated in two ways: 1) with Eqs. (4) or (5) and 2) through calorimetry experiments. Variable ΔQ_S was computed from the NYSDOT concrete temperature data collected during the field projects:

$$\Delta Q_S = \rho_c c_{pc} \Delta Z_c \left[\sum_{zc=1}^{nz} \frac{\Delta \overline{T}(zc)}{\Delta t}\right]. \quad (21)$$

An area-weighted average of energy storage over the form and over the beams was used to account for spatially variable temperatures. The estimated Q_I from the balances was compared with that from calorimetry experiments.

3. Results

The thermal conductivity, heat capacity, and density of class-HP concrete are discussed first. Next, the energy balances for the 1999 bridge are presented because it provides the most complete description of a bridge–atmosphere system to date. Last, the energy balances of the four bridges are compared and estimates of Q_I are determined.

a. Properties of class-HP and class-H concrete

From laboratory tests on a class-HP concrete sample from the 1999 bridge, the density is 2230 kg m^{-3} and specific heat capacity is 1380 J kg^{-1} K^{-1} with individual tests giving a range from 1300 to 1450 J kg^{-1} K^{-1} (Wojcik et al. 2001, manuscript submitted to *Cem. Concr. Res.*). We believe this sample is representative of the entire bridge because the concrete mix design was constant from truck to truck and all the concrete came from the same supplier. While these properties

Unauthenticated | Downloaded 02/24/21 06:32 PM UTC

vary depending on the materials used, especially aggregate, the estimated values are reasonable in comparison with published ranges of 2000–2400 kg m^{-3} and 900–1800 J kg^{-1} K^{-1}, respectively (Scanlon and McDonald 1994). Because the bridges used similar mix design and because the coarse aggregate was similar (dolomite and limestone), the 1999 values were used for the other bridges.

The concrete thermal conductivity was estimated with the heat flux plates and the 1D model. The data from heat flux plate 2 were unrealistically small, perhaps because of instrument failure or because it was not level in the concrete. They were not considered in our k_c estimates. Because plate 1 has a thermal conductivity of 1.22 W m^{-1} K^{-1} and because we believe the actual k_c to be between 2 and 4 W m^{-1} K^{-1}, the plate disrupted the ''normal'' heat flow in the measurement area. Therefore, the plate's Q_{GA} values were corrected based on the plate diameter and thickness and the plate and concrete thermal conductivities as suggested by Philip (1961). Based on the corrections, measured plate-1 Q_{GA} could be too low by 15% if $k_c = 2$ and by 44% if $k_c = 4$. To select our estimated k_c, an iterative approach was used in which a value of k_c was selected and the appropriate correction factor was applied to the plate data. The final value selected as k_c for the 1999 bridge was that with which the corrected plate data matched Q_{GA} from the temperature gradient and the guessed k_c. This procedure yielded $k_c = 2.5$ W m^{-1} K^{-1}.

The 1D model suggested $k_c = 2.8$ W m^{-1} K^{-1} provides the best predictions of the observed vertical temperature differences. The average value of the estimates was about 2.7 W m^{-1} K^{-1}, and so this was the value selected for k_c for the 1999 bridge. For the other bridges, because of lack of data, the only method employed was the model. For the 1998, 1996, and 1995 bridges, the conductivities are 3, 2.7, and 3.1 W m^{-1} K^{-1}, respectively.

b. 1999 bridge

From 10 to 14 June 1999, the weather near Amsterdam, New York, was dominated by clear skies and light winds for the first three days and nights, with partly cloudy skies on the final day and night (Table 1). Afternoon temperatures approached 30°C and nighttime temperatures dropped to as low as 9°C. Afternoon relative humidities were around 40% and night values approached 100%. Winds were less than 1.5 m s^{-1} during the day and less than 1 m s^{-1} at night.

The pour began at 0700 LT on 10 June and concrete reached the NYSDOT thermocouples by 1000 LT. With solar heating, the top surface temperatures climbed to almost 30°C by the late afternoon while temperatures deeper in the slab reached almost 25°C (Fig. 5). By the evening, the hydration reactions began in earnest (stage 3) and led to peak concrete temperatures near midnight. At this time, the highest temperatures occurred at the top of the form (43°C) and the lowest at the top surface (29°C). During 10–11 June, the top surface exhibited a double peak in its temperature—the first from the normal afternoon solar heating and the second due to the chemical heat source. The temperature gradient near the top of the concrete was about 3°C $(27\ mm)^{-1}$, while that just above the form was less than 0.5°C $(27\ mm)^{-1}$, suggesting that most heat exchange with the bridge deck occurred at the top surface. During 12–14 June, the bridge increasingly became a passive participant in its environment as its internal heat source waned, allowing solar heating and local surface fluxes to determine the concrete temperatures.

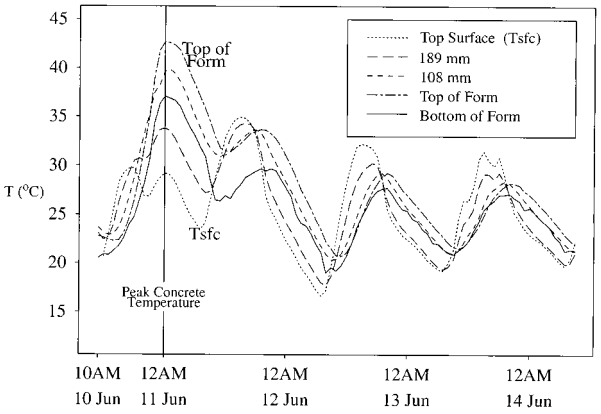

FIG. 5. Hourly averaged concrete and form temperatures measured at the 1999 bridge. The labeled distances are distances up from the top of the form (within the concrete). The top surface (Tsfc) concrete temperature was taken at approximately 243 mm above the form. The ''Top of Form'' temperature was taken on the concrete side of the form, while the ''Bottom of Form'' temperature was taken on the exposed side of the form.

1) TOP SURFACE LATENT AND SENSIBLE HEAT FLUXES (Q_{HA} AND Q_{EA})

To properly estimate the top surface convective fluxes, we considered several issues. First, we determined the vertical gradients of temperature and humidity. Since the vertical gradients we computed used a surface value and an air value (see section 2c), we found what surface measurements were the best suited for this task. Next, we determined how the development of the IBL over the bridge influenced the air temperature, humidity, and wind speed and compared values from the IBL with those from the tower. Last, through the footprint analysis, we determined to what extent the eddy flux measurements were influenced by the bridge's top surface. Our process of addressing these issues is discussed below.

(i) Vertical gradients and the IBL

The relevant surface temperature for computing Q_{HA} and Q_{EA} is the ''skin'' temperature of the burlap covering

Unauthenticated | Downloaded 02/24/21 06:32 PM UTC

the curing concrete. At the 1998 bridge, skin temperature variations across the bridge's top surface, with extremes as large as 6°C, were on average less than 3°C as indicated by thermal images (Wojcik 2001). These data, then, suggest that point measurements with an infrared thermometer can adequately describe the skin temperature of the entire deck.

During the night at the 1999 bridge, the skin temperatures measured with an infrared thermometer were within about 1°–2°C of the top surface concrete temperatures (under the burlap, measured with the thermistors and NYSDOT thermocouples). Daytime infrared measurements were compromised by shadows in the field of view of the instrument. Therefore, during the daytime, the average of all top surface concrete measurements (thermocouples and thermistors, excluding the infrared measurement) was used as an estimate of the skin temperature, while the skin temperatures from the infrared thermometer were used during the night. For the 1999 bridge, use of the concrete temperatures instead of the infrared (unrepresentative) skin temperatures during the day raised BR Q_{EA} estimates by $<$ 25% and lowered BR Q_{HA} estimates by $>$ 40%, respectively, although Q_{HA} was small [less than 45 W m^{-2}; see section 3b(1)iii].

Differences in wind speeds measured with the Applied Technologies, Inc. (ATI) sonic anemometer over the bridge and those measured on the tower with the Gill propeller anemometer were no more than 0.3 m s^{-1} and generally 0.1 m s^{-1} or less. Such small variation would make a negligible difference in the computed fluxes.

Large temperature and humidity differences were present between the surface and 0.6 m (7°C and 14 g kg^{-1}, larger values at the surface) during afternoon periods, but no measurements were taken between these levels. Daytime specific humidities at 0.6 and 1.4 m (Vaisala Humitters) and at 0.9 m (Krypton hygrometer) above the deck were consistently 1.5–2.1 g kg^{-1} higher than those values from the tower (CS500), which we assume were representative of conditions upwind of the bridge. These differences were much larger than the instrument accuracies ($\pm$0.4 g kg^{-1}) and indicate some influence of the bridge at least to a height of 1.4 m. Temperature differences among these levels were less than 0.2°C, much smaller than the instrument accuracies ($\pm$0.6°C).

The temperature and humidity comparisons suggest that the IBL reached to at least 1.4 m, but the influence of the bridge's top surface is small at these levels. The differences in the temperatures, humidities, and wind speeds from the tower (CS500) as compared with the IBL values would make $<$ 10% difference in flux-gradient estimates of Q_{HA} and Q_{EA} [see section 3b(1)iii]. Therefore, measurements of temperature, humidity, and wind speeds directly over the bridge's top surface seem unnecessary to estimate fluxes with the flux-gradient approaches if measurements near the bridge are taken.

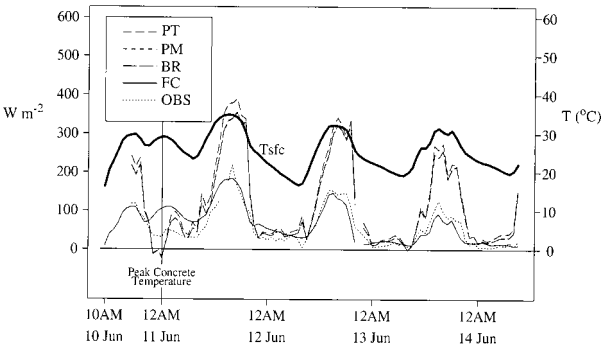

FIG. 6. Estimates of Q_{EA} for the 1999 bridge. Labels PT, BR, and PM are estimates from, respectively, the Priestley–Taylor, Bowen ratio, and Penman–Monteith methods. Here, FC uses free convection exchange coefficients from Kondo and Ishida (1997) for a smooth surface, while OBS is the measured direct eddy flux Q_{EA}. The heavy solid line (Tsfc) is the top surface concrete temperature. Note that BR and PM values are almost identical.

(ii) Measured Q_{HA} and Q_{EA} and the flux footprint

In making direct eddy flux measurements over the bridge, several procedural issues arose: 1) sampling frequency, 2) height of the instruments, and 3) the separation of the ATI sonic anemometer and the krypton hygrometer (for Q_{EA}). First, the relatively low sampling frequency (1-Hz grab samples), through aliasing, still allowed us to get an adequate estimate of fluxes even without being able to resolve higher frequencies. Second, while it is often suggested that the ATI sonic anemometers not be used below a height of 4 m for adequate flux estimates (e.g., Kaimal and Finnigan 1994, p. 219), Kristensen and Fitzjarrald (1984) pointed out that adequate flux measurements can be made at heights of 4–5 times the anemometer pathlength. With a pathlength of 15 cm, the ATI anemometer can be used for accurate flux measurements as low as 0.6 m, even lower than the level of our measurements (0.9 m). Last, the ATI anemometer and the krypton hygrometer were positioned 50 cm apart, which could produce underestimates of Q_{EA} of about 10%–15% by decorrelating the measurements of q and w (Laubach and McNaughton 1998). Kristensen et al. (1997) suggested placing the hygrometer below the anemometer when sampling close to the ground to limit this problem, though this was not feasible at the 1999 bridge.

The power spectra for high-frequency w, T, and q were similar to the hypothesized surface layer spectra with MOSH scaling as given by Kaimal et al. (1972). The measured convective fluxes were within 10%–15% of those values obtained by integration of the surface layer MOSH cospectra predictions. These findings suggest that the measured fluxes were not erroneous because of instrument or sampling troubles.

The eddy flux measurements made at 0.9 m were taken within the IBL during the day and were influenced

Unauthenticated | Downloaded 02/24/21 06:32 PM UTC

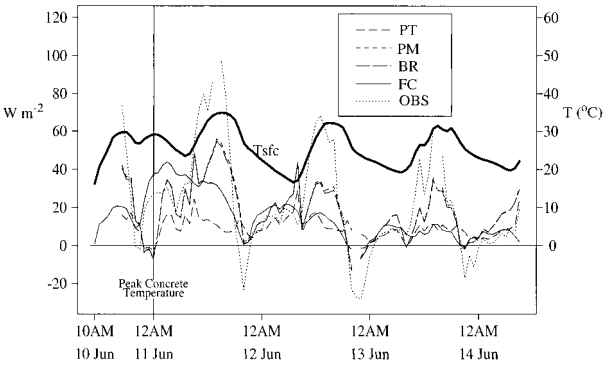

FIG. 7. Estimates of Q_{HA} for the 1999 bridge. The measured direct eddy flux Q_{HA} is labeled as OBS. See Fig. 6 for definition of other labels. Note that BR and PM values are almost identical.

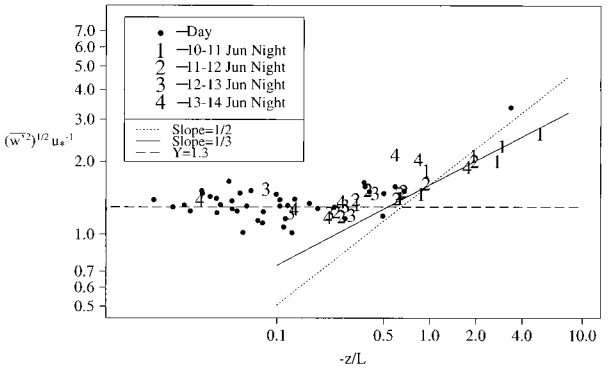

FIG. 8. Hourly averaged values of the measured root-mean-square vertical velocity perturbations scaled by the friction velocity (u_*) against $-z/L$ for the 1999 bridge.

by the top surface. The measured peak Q_{EA} and Q_{HA} decreased each subsequent day (Figs. 6 and 7), as did the top surface temperatures as the internal heat source decreased with time. The upwind surface conditions probably did not change during this period because atmospheric conditions were similar each day (sunny, light winds) and so cannot be the cause of the temporal decrease in the measured peak fluxes. Also, histograms of high-frequency w, and in particular, T and q show positive skewness over much of the period, indicating convective conditions (Chiba 1978), as would be expected from the bridge's top surface.

For the 1999 bridge, the wind blew along the length of the bridge (Fig. 3), providing the best fetch possible. According to the Horst and Weil footprint model, at a fetch of 16 m from the leading edge of the bridge and at a measurement height of 0.9 m, 26% of the measured fluxes could be attributed to the bridge with the rest from the upwind area when considerable horizontal advection is occurring (mostly during the afternoon periods at the 1999 bridge). The cospectra also suggest that up to 90% of the measured sensible and latent heat fluxes was attributed to eddies larger than the length of the fetch (16 m). In other words, up to 90% of the observed fluxes is attributed to areas upwind of the bridge. The footprint prediction and the observed cospectra underscore the difficulty in relating directly measured eddy fluxes over a small area such as the bridge to the actual surface fluxes.

(iii) Estimated Q_{HA} and Q_{EA}

Data collected at the 1999 bridge indicate an IBL during the daytime. The differences in temperature, humidity, and wind speed values in the IBL and those at the tower make only small differences in the computed fluxes with the flux-gradient methods. For the 1999 analysis below, we chose to use the air temperature and humidity measured with the Humitter at 0.6 m and wind speed values measured with the ATI sonic anemometer mounted on booms over the bridge. The surface values for temperature and humidity (assumed to be the saturated value at the surface temperature) came from the thermistors and thermocouples under the burlap during the day and from the infrared thermometer during the night (Fig. 3 and Tables 2 and 3).

The BT method with free convection exchange coefficients for a smooth surface (FC) and the BR, the PM, and the PT methods were used to estimate Q_{EA} and Q_{HA}. To determine when free convection conditions existed above the bridge, the fast-response data were compared with an extension of MOSH under free convection conditions as given by Wyngaard et al. (1971):

$$\frac{(\overline{w'^2})^{1/2}}{u_*} = G\left(-\frac{z}{L}\right)^{1/3}, \tag{22}$$

where G is a proportionality constant that Wyngaard et al. (1971) suggested is ~1.9. At the 1999 bridge, when $-z/L > 2$, the vertical velocity perturbations show roughly a $(-z/L)^{1/3}$ dependence, suggesting the presence of free convection (Fig. 8). Most points found at $-z/L > 2$ occurred during the night of 10–11 June when the surface–air ($z = 0.6$ m) temperature difference was between 10° and 15°C and wind speeds were < 0.5 m s^{-1}. These same atmospheric conditions indicate that during this night, the air sampled by the fast response instruments was more representative of the bridge than during periods with stronger winds (>1 m s^{-1}) and greater stability. The calm conditions and clear skies during that night suggest that a typical stable layer encompassed the region. These free convection conditions measured over the bridge, then, developed in part because of the concrete's hydration heat source.

During the night of 10–11 June, Q_{EA} estimates ranged from 0 to about 110 W m^{-2} (Fig. 6). During the following day, the BR, PT, and PM approaches indicated that Q_{EA} was between 350 and 400 W m^{-2} at its middle afternoon peak. However, the measured value peaked at about 220 W m^{-2}, with which the FC estimate is in close agreement. These comparisons hold throughout the period as the estimates converge at night and show

Unauthenticated | Downloaded 02/24/21 06:32 PM UTC

TABLE 4. Estimated uncertainties of the energy balance terms and concrete properties for the 1999 bridge. These uncertainties were determined by considering a combination of instrument accuracies, datalogger sampling frequency and conversions, mounting problems of the instruments, and on other estimates of the given term.

Term	Uncertainty
Q_{GA}	30%
Q_{RA}	25%
Q_{EA}	50%
Q_{HA}	50%
Q_A^*	15%
Q_{GB}	50%
Q_B^*	50%
Q_{HB}	20%
Q_I	20%
ΔQ_S	<10%
c_{pc}	<10%
ρ_c	<1%
k_c	30%

a large disparity during the day, with the measured and free convection values being a factor of 1.5 smaller than the other estimates.

The Q_{HA} estimates also converge during the night and show large scatter during the day (Fig. 7). During the night of 10–11 June, the measured Q_{HA} peaked at about 30 W m^{-2}, with all other estimates within 25 W m^{-2} of this value. During the daytime, however, the measured Q_{HA} was about 1.5–6 times greater than the other estimates.

The disparity between our flux measurements and the other estimates of convective fluxes is not attributed to our sampling rate of 1 Hz or the height of our flux sensors (0.9 m), as discussed in section 3b(1)ii. Also, the distance between the ATI sonic anemometer and krypton hygrometer may lead to errors in the Q_{EA} eddy flux estimates of up to 15% [see section 3b(1)ii], much less than the differences between the eddy flux estimates and the energy balance estimates. The disparity, then, indicates that at 0.9 m above the bridge at a fetch of 16 m, the IBL that developed probably still carried with it turbulence and scalar characteristics of the upwind surfaces and source areas. This finding emphasizes the need for understanding the interaction of step changes in surface fluxes, surface roughness, and entrainment in IBL development and how this interaction influences the footprint of scalar concentrations, vertical scalar profiles, and direct eddy flux measurements over small areas.

During the afternoon of 11 June, measured Q_{EA} was 220 W m^{-2} (Q_{HA} = 90 W m^{-2}) and the BR estimate of Q_{EA} was 360 W m^{-2} (Q_{HA} = 50 W m^{-2}). The footprint model with a formulation for the case of a general step change in surface flux was given by Horst and Weil (1994). The model suggests that if the BR fluxes are assumed to be accurate, the upwind Q_E was 170 W m^{-2} (Q_H = 110 W m^{-2}). These upwind flux estimates are consistent with the upwind surfaces, which include (from the most distant to closest to the bridge) fields, lawns, and 100 m of asphalt. During this same afternoon, given the BR fluxes, a parcel of air with a depth of 1.5 m traveling over the bridge to the measurement location would moisten on average by about 1.1 g kg^{-1} and would warm by 0.4°C, consistent with the measured differences from above the deck to the tower.

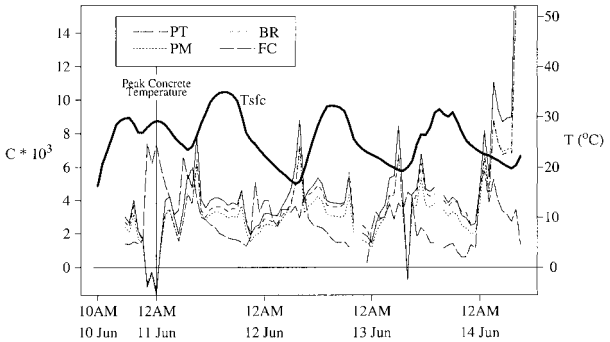

FIG. 9. Exchange coefficients ($C \times 10^3$) for the 1999 bridge. See Figs. 6 and 7 for explanation of labels.

The estimates of the BR, PM, and PT Q_{EA} and Q_{HA} are dependent on Q_{GA}, which is dependent on k_c. If k_c = 3 W m^{-1} K^{-1}, Q_{EA} and Q_{HA} increase by no more than 25% during most time periods over the values when k_c = 2.7 W m^{-1} K^{-1}. The measured fluxes and sensitivity of Q_{EA} and Q_{HA} to k_c suggest an uncertainty of no larger than 50% in our estimates of Q_{EA} and Q_{HA} (Table 4).

(iv) Exchange coefficients

By equating the above flux estimates to the BT formulations Eqs. (15) and (16), exchange coefficients were determined for a reference height of 0.9 m. The estimated exchange coefficients showed a diurnal variation with larger values during the day (Fig. 9). While they were as large as 0.015 around sunrise and sunset, they ranged from 0.0015 to 0.005 over most time periods, in reasonable agreement with other published results (e.g., Arya 1977; Stull 1988; Garratt 1992). The drag coefficient from the fast-response measurements was larger than the exchange coefficient estimates by a factor of 20 or more during the afternoon periods. These coefficients as estimates of C_h or C_e would give unrealistic flux estimates but were consistent with the rougher areas upwind of the bridge from where almost 75% of measured fluxes came, according to the footprint analysis.

2) RUNOFF WATER HEAT FLUX (Q_{RA})

The term Q_{RA} was computed with two different values for the initial water temperature as the drops hit the top surface: 1) drop temperature was the wet-bulb temperature of the air and 2) drop temperature adjusted to its environment as given by the Pruppacher and Klett model. Assuming that the drops reached the wet-bulb temperature of the air provides an upper limit to the heat

Unauthenticated | Downloaded 02/24/21 06:32 PM UTC

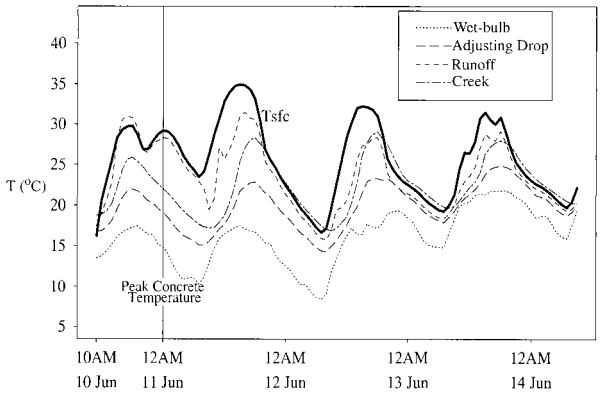

FIG. 10. Measured and estimated water temperatures for the 1999 bridge. The ''Wet-bulb'' temperature is the wet-bulb temperature of the ambient air. The ''Creek'' temperature is the water temperature beneath the bridge, which was used as spray water on the bridge's top surface. The ''Runoff'' temperature was measured with a thermistor at the northeast corner of the bridge where water ran off (Fig. 3). The ''Adjusting Drop'' temperature is the average temperature of the spray water as it hit the top surface, having traveled approximately 4 m through the air, as determined with the Pruppacher and Klett (1997) model. The heavy solid line (Tsfc) is the top surface concrete temperature.

removed by the runoff water. We note that the runoff water temperature during the daytime was as much as 6°C lower than the top surface temperature (Fig. 10). We believe that the water running off the bridge where we placed the thermistor did not provide a representative sample of the overall runoff water temperature because of the geometry of the bridge, placement of hoses, and the partial shading of the deck surface by construction equipment. Therefore, to compute Q_{RA}, we assumed that T_{wf} was equal to the top surface temperature instead of the measured runoff water temperature.

During the night, the adjusting drop temperature was as much as 7°C larger than the wet-bulb temperature (Fig. 10). Given this temperature difference, if the wet-bulb scenario is assumed, Q_{RA} would be from 10 to 80 W m^{-2} higher (>25%) than that from the adjusting drop scenario. For example, during the night of 10–11 June, the wet-bulb Q_{RA} = 200 W m^{-2} and the adjusting drop Q_{RA} = 150 W m^{-2}. Although the exact runoff flow rate is not known, the water balance estimates suggest that 95% or more of the water sprayed onto the bridge ran off (discussed in section 3c). We believe that our adjusting drop estimate of Q_{RA} has an uncertainty of 25% (Table 4).

3) TOP SURFACE NET RADIATION (Q_A^*)

To estimate the uncertainty of the Q_A^* measurements, the measured values were compared with those computed by using the individual longwave and shortwave terms of the net radiation. The incoming shortwave radiation was measured. To estimate the reflected shortwave, the albedo of the bridge top (0.14 for wet burlap covering concrete) was determined with an albedometer. To estimate the outgoing longwave radiation, Stefan–Boltzmann law was used with a wet burlap emissivity of 0.98 and the bridge's top surface temperatures. To estimate the incoming longwave radiation, Stefan–Boltzmann law was used with the air temperatures and air emissivities computed with schemes proposed by Geiger (1965) and another by Idso (1981), both of which determine the longwave emission of air with the air vapor pressures and temperatures. The incoming longwave scheme developed by Prata (1996) was also used. The estimated Q_A^* values were within ±15% of the measured values, or no more than ±60 W m^{-2} over most of the period. Therefore, the measured Q_A^* is reliable, with an uncertainty of 15% (Table 4).

4) TOP SURFACE CONCRETE HEAT FLUX (Q_{GA})

Term Q_{GA} was bounded from Eq. (5) with the maximum and minimum likely c_{pc} for ΔQ_S in Eq. (21), the maximum and minimum calorimetry estimates of Q_I (see section 3d), and maximum and minimum Q_{GB} [see section 3b(6)]. During the night of 10–11 June, Q_{GA} was between 320 and 420 W m^{-2}. Given k_c = 2.7 W m^{-1} K^{-1}, Q_{GA} from Eq. (20) was about 350 W m^{-2} at its peak, within the bounded range. During nighttime periods later in the project when the concrete was generating little heat, Q_{GA} approached 120 W m^{-2}, with a range of values from 80 to 140 W m^{-2}. Daytime values approached 300 W m^{-2} later in period. Given the uncertainties in k_c and c_{pc}, Q_{GA} has an uncertainty of 30% (Table 4).

5) 1999 TOP SURFACE ENERGY BALANCE

To construct the complete top surface energy balance, Q_{EA} and Q_{HA} were estimated with the BR approach, which is in agreement with PM and PT methods. Variable Q_{GA} was computed with k_c = 2.7 W m^{-1} K^{-1}, c_{pc} = 1380 J kg^{-1} K^{-1}, and Eq. (18). Term Q_{RA} came from the adjusting drop procedure. The net radiation flux Q_A^* was determined from our measurements. During the period of peak heat loss on the night of 10–11 June, the top surface of the concrete lost about 350 W m^{-2} (Fig. 11). The dominant heat removal mechanism was Q_{RA}, which removed about 150 W m^{-2}. About 90 W m^{-2} was removed by Q_A^*, about 80 W m^{-2} by Q_{EA}, and about 35 W m^{-2} by Q_{HA}. During the more passive nighttime hours later in the period, Q_{GA} was about 120 W m^{-2}, most of which was lost through Q_A^* as the other balance terms approached zero. Note that because atmospheric conditions during each night were similar, the hydration heat source produced the higher nighttime flux values on the night of 10–11 June as compared with those during the more passive nights later in the period.

At around noon on 11 June, some of Q_A^* (600 W m^{-2}) went into heating the concrete (160 W m^{-2}) and the rest was lost to Q_{EA} (200 W m^{-2}), Q_{RA} (200 W m^{-2}),

Unauthenticated | Downloaded 02/24/21 06:32 PM UTC

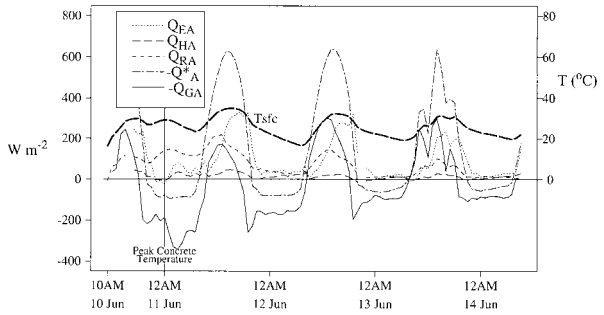

FIG. 11. Hourly averaged top surface energy balance terms for the 1999 bridge with Q_{EA} and Q_{HA} given by the BR approach, Q_{RA} given by the adjusting drop procedure, measured Q^*_A, and Q_{GA} with k_c = 2.7 W m^{-1} K^{-1}. The bold dashed line (Tsfc) indicates the top surface concrete temperatures.

and Q_{HA} (40 W m^{-2}). The daylight hours of 11 and 12 June experienced very similar ambient conditions: light winds and clear skies. However, about 140 W m^{-2} more was absorbed by the concrete at around noon on 12 June than on 11 June. On 11 June, the concrete surface temperatures were about 3°C higher than those on 12 June because the concrete had just completed stage 3. The higher top surface concrete temperatures on 11 June enhanced Q_{EA}, Q_{HA}, and Q_{RA}. Thus, Q_{GA} was smaller.

6) HEAT EXCHANGE FROM THE BRIDGE BOTTOM

The total heat loss from the bridge bottom peaked at about 55 W m^{-2} during the night of 10–11 June, mostly due to conduction down the beams and net radiation (Figs. 12a and 13a). Heat loss from the beams resulted in the formation of a stable layer [23°C (0.9 m)$^{-1}$] between the beams (Fig. 13b). Conductive and aerodynamic heat loss from the form was small (<5 W m^{-2}) because the stable layer of air between the beams restricted mixing near the form and because the form is partially insulated. Heat lost as net radiation peaked at 25 W m^{-2} and had contributions from both the form and steel support beams. The emissivity of the shiny metal form is small ($\varepsilon \cong 0.1$–0.15) and although the form temperatures reached 38°C, the form contribution to Q^*_B was small. Much of Q^*_B came from the adjacent oxidized steel support beams ($\varepsilon \cong 0.80$). Very small temperature gradients immediately above the form were consistent with these findings.

The heat loss from the beams amounted to about 30 W m^{-2} when scaled to the area of the bridge because the beams are only in contact with about 20% of the bottom surface of the concrete. Locally, the beams removed roughly 150 W m^{-2} just above them, which produced horizontal concrete temperature gradients. In fact, top surface temperatures directly above a beam were consistently 2°–3°C cooler than those directly above the form during the night of 10–11 June.

The amount of heat lost from between the beams, as measured with the 1D sonic anemometer/fine wire thermocouple (Fig. 12b), was much less than would be expected if the heat conducted down the beams was dissipated to the air between the beams and then eventually mixed away. This discrepancy arises because in the estimate of Q_{GB}, beam heat loss was counted twice as some of the heat conducted down the beams contributed to Q^*_B. The balance estimate and the measured heat transfer between the beams suggest that heat exchange from the bridge bottom was no more than 55 W m^{-2} during stage 3 and no more than ±25 W m^{-2} during the more

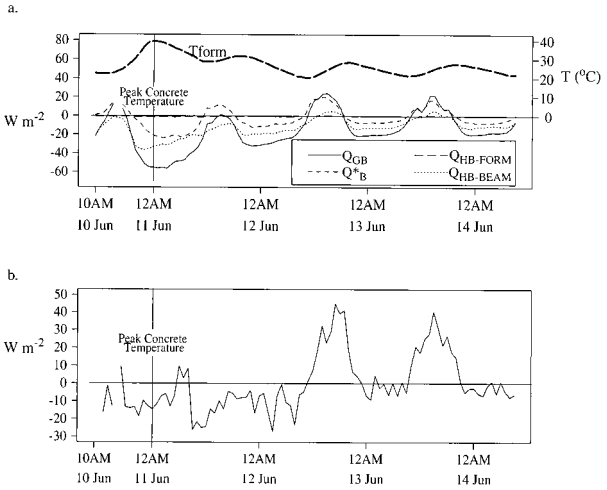

FIG. 12. (a) Hourly averaged bottom surface energy balance for the 1999 bridge: $Q_{H\text{-}BEAM}$ is the amount of heat transferred vertically through the beam by conduction; $Q_{H\text{-}FORM}$ is the amount of heat transferred vertically through the form. The heavy dashed line is the temperature of the bottom surface of the form (Tform). (b) Measured heat transferred from between the beams to the ambient environment.

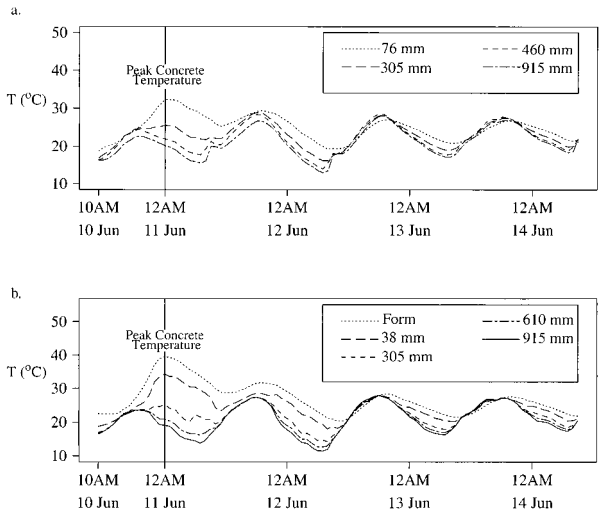

FIG. 13. (a) Hourly averaged support beam temperatures from the 1999 bridge. Labeled distances are distances of the measurement (indicated by H in Fig. 4) down from the top of the beam. (b) Hourly averaged air temperatures between the support beams for the 1999 bridge. Labeled distances indicate the distance of the measurement (indicated by G in Fig. 4) down from the bottom of the form.

Unauthenticated | Downloaded 02/24/21 06:32 PM UTC

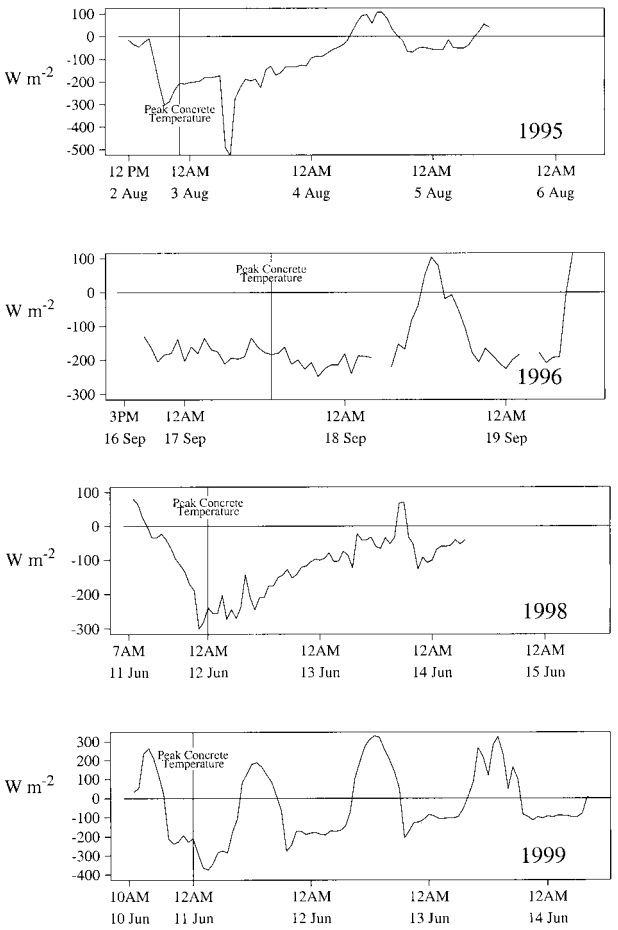

FIG. 14. Comparison of $-Q_{GA}$ for the four bridges. Note that the scales of the axes for each bridge are different.

passive periods, or 15% of Q_{GA}, with an uncertainty of 50% (Table 4).

c. Comparison of bridge energy balances

For the 1995, 1996, and 1998 bridges, Q_{EA} and Q_{HA} were estimated with the BR approach with air measurements of temperature, humidity, and wind speed taken on the towers nearby (Table 1). Recall that our analysis from the 1999 bridge suggested that measurements from the tower (which we assume were not influenced significantly by the bridge surface) provided adequate air data to determine the surface convective fluxes from the bridge's top surface [see section 3b(1)i]. Note that the winds for the 1995 and 1996 bridges generally blew across the shortest dimension of the bridges, while for the 1998 bridge, the winds blew along the longest axis of the bridge.

No source water or runoff water temperatures for the 1996 and 1995 bridges were measured. The water temperature, as it hit the top surface for these bridges, was assumed to be the air's wet-bulb temperature, while noting the potential biases this assumption may introduce

TABLE 5. Average top surface energy balance terms (W m^{-2}) and peak concrete temperatures for each bridge during a 5-h period around the time of the maximum concrete temperatures. Energy balance terms are from the BR approach.

	1995	1996	1998	1999
$-Q_{GA}$	−209	−172	−247	−286
Q_{RA}	0	125	23	136
Q_{EA}	87	54	138	43
Q_{HA}	54	22	60	18
$-Q_A^*$	−68	30	−24	−87
Peak concrete temperature	55°C	31°C	37°C	43°C

[see section 3b(2)]. The runoff water temperatures were assumed to be the top surface temperature. For the 1995 bridge, the spray water volume was that which closed the top surface balance with $k_c = 3.1$ W m^{-1} K^{-1} to compute Q_{GA}.

For the 1998 and 1999 bridges, a distinct peak in the top surface heat loss occurred near the time of peak concrete temperatures, because heat was continually removed throughout these nights (Fig. 14 and Table 5). The peak heat loss at the 1999 bridge occurred several hours after the peak concrete temperatures, when after a few hours of almost no wind, wind speeds increased, providing more efficient heat loss from Q_{EA} and Q_{HA}. The lack of a distinct maxima in Q_{GA} at the time of peak concrete temperatures at the 1996 bridge was the result of more retarder in the mix for this bridge than the others, which led to slower hydration rates (Table 1). A failed generator at the 1995 bridge resulted in no spray water during stage 3 (night of 2–3 August) and, with light winds, heat loss was limited to about 210 W m^{-2}. With no spray water, the top surface was no longer saturated. To account for this in the BR approach, we assumed that q_s was one-half of the saturation value at the top surface temperature as evaporation from the concrete itself occurred. By the following morning when the water was turned on again, about 500 W m^{-2} was removed for 2 h.

During stage 3, Q_{RA} was the dominant heat loss term for the 1996 and 1999 bridges, because wind speeds were light and evaporation was small. Evaporation heat flux Q_{EA} was dominant for the 1998 and 1995 bridges (Table 5). The 1998 bridge experienced higher wind speeds (>1 m s^{-1}) than did the 1996 and 1999 bridges (<1 m s^{-1}) and so evaporation was enhanced. With top surface temperatures approaching 43°C and no spray water at the 1995 bridge, evaporation from the concrete itself dominated the top surface balance. The top surface heat transfer and the concrete temperatures, then, can depend on atmospheric conditions, construction practices, and the concrete mix design.

Because the average measurement height varied from bridge to bridge (Table 1), the exchange coefficients for each bridge are not directly comparable to each other until they are scaled by height. We scaled the coefficients for the 1995, 1996, and 1998 bridges to a ref-

Unauthenticated | Downloaded 02/24/21 06:32 PM UTC

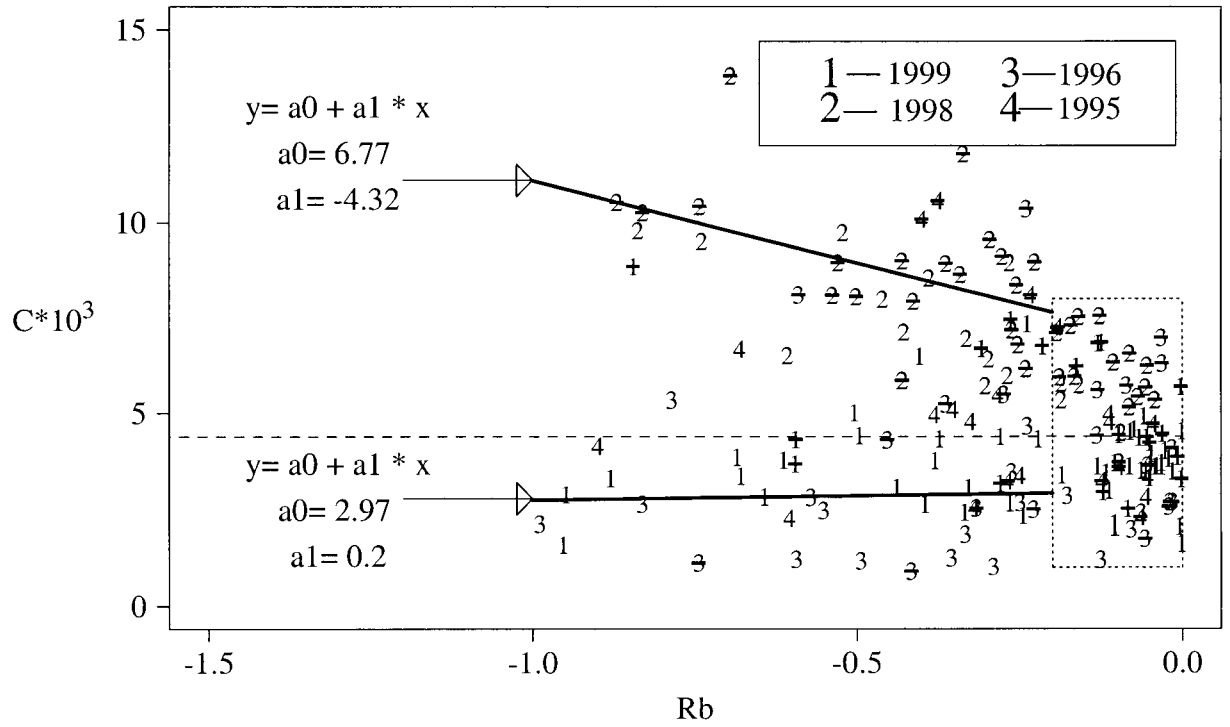

FIG. 15. Exchange coefficients ($C \times 10^3$) vs bulk Richardson number (Rb) for the four bridges. The points in the box made by the dotted lines were used to determine the average exchange coefficient for Rb > -0.2, indicated as the dashed line at $C \times 10^3 = 4.4$. The numbers with a dash through them indicate values when the surface to air virtual temperature difference ($T_{sv} - T_{av}$) was < 5°C. The two bold solid lines were determined with linear regression for Rb < -0.2. The upper line was determined for those points with $T_{sv} - T_{av} < 5$°C and the lower line for $T_{sv} - T_{av} > 5$°C.

erence height of 0.9 m (1999 bridge). To do this, we used MOSH expressions for exchange coefficients (e.g., Garratt 1992) with several stability values ($-300 < -z/L < 0$) and roughness lengths (0.001 m $< z_0 <$ 0.01 m). A ratio of the 1999 MOSH exchange coefficients to those of the other bridges indicated that, on average, the 1995, 1996, and 1998 exchange coefficients needed to be increased by a factor of roughly 1.4 to be valid at $z = 0.9$ m. We realize that MOSH may not be applicable to the small, heterogeneous bridge environment, but we feel it can provide a rough estimate of the needed scaling factor.

We relate the scaled BR exchange coefficients from the four bridges to the bulk Richardson number (Rb):

$$\text{Rb} = g\Delta\overline{\Theta}_v z/[\overline{\Theta}_v(U)^2]. \quad (23)$$

See the appendix for definitions of variables. By using Rb as the independent variable for the analysis, the exchange coefficients are directly related to easily observable variables: wind speeds and surface and air temperatures and humidities. Because there were few data points for Rb < -1, the analysis was performed only for Rb > -1.

There is much scatter in the exchange coefficient data, but most points were located at Rb > -0.2 (Fig. 15). The average of these points is $C = 0.0044$, with a standard deviation of 0.0015. Exchange coefficients used by Plawsky and Kapila (1997) were generally 1.5–2.5 times lower than these values.

At Rb < -0.2, we note two populations of points. Those points below $C = 0.0044$ do not vary much with Rb while those above $C = 0.0044$ increase with decreasing Rb. When we further divide the points by the surface-to-air virtual temperature difference ($T_{sv} - T_{av}$), we find that most of the points for $C > 0.0044$ occur when $T_{sv} - T_{av} < 5$°C and those at $C < 0.0044$ occur when $T_{sv} - T_{av} > 5$°C. As air flowed from the rougher upwind areas to the smoother bridge, the production of mechanical turbulence decreased. In the more buoyant cases, the mechanical turbulence was dissipated as the thermally generated turbulence began to dominate, resulting in lower exchange coefficients. The exchange coefficients in the less buoyant situations were larger because, with less thermal convection, the mechanical turbulence was not dissipated as rapidly. Note that if $z_0 = 0.01$ m, MOSH provides roughly the same magnitude of C and variation of C with Rb as the observed less buoyant points for $-1 <$ Rb < -0.2.

These findings are consistent with those from Andreas and Cash (1999) for IBLs over convective Arctic leads and polynyas where mechanically generated turbulence was slowly overcome by thermally generated turbulence as the fetch increased. At smaller fetches, the combination of free and forced convection resulted in larger

Unauthenticated | Downloaded 02/24/21 06:32 PM UTC

exchange coefficients than those at greater fetches when thermal forces dominated. In our data, when buoyancy forces were smaller ($T_{sv} - T_{av} < 5$°C), exchange coefficients were larger than those during the more buoyant periods as mechanical mixing dominated.

With $T_{sv} - T_{av} = 13$°C (a typical value from our stage-3 bridge data), Rb $= -1$, and $U = 1$ m s^{-1} (the latter two chosen as the typical cutoffs for free convection), our data suggest $C = 0.0028$ or $CU = 0.0028$. To compare this value with the Kondo and Ishida (1997) smooth surface free convection prediction of CU, we scaled their value from their reference height (1.5 m) to ours (0.9 m) by multiplying their value for CU by $(1.5/0.9)^{1/3} = 1.19$ for free convection scaling as suggested by Wyngaard et al. (1971). This procedure gives $CU = 0.0031$, for the same temperature and stability conditions, which is in close agreement with our data.

Therefore, we recommend $C = 0.0044$ be used when Rb > -0.2 while noting the standard deviation in C of 0.0015. For Rb < -0.2, our data suggest $C > 0.0044$ when $T_{sv} - T_{av} < 5$°C and $C < 0.0044$ when $T_{sv} - T_{av} > 5$°C. Because of our limited data, the coefficients from our data for Rb < -0.2 must be used with caution.

For the 1999 bridge, 3.7 m^3 h^{-1} of water were sprayed on the bridge, while at most 0.15 m^3 h^{-1} evaporated (<5%). For the 1998 bridge, less than 10% of the spray water evaporated. Since Q_{RA} was much smaller than Q_{EA} for the 1998 bridge (Table 5) and since excess water was pumped onto the bridge, the abundant precipitation that fell during this project, which was roughly one-third of the total water incident on the bridge, had little effect on the overall heat balance.

Heat transfer at the bridge bottom surfaces was at most 15% of that transferred through the top for the 1998 and 1999 bridges. For the 1996 bridge, bottom heat transfer was about 30% of the top value, larger than that for the more recent bridges. The 1996 beam tops have a larger surface area in contact with the concrete, and so they removed heat more efficiently. Sufficient data were not available to estimate the 1995 bottom heat transfer. However, because its structure is similar to that of the 1998 and 1999 bridges, we believe that the 1995 bottom heat transfer was at most 15% of the top heat transfer.

d. Hydration heat source

With the estimates of the top and bottom surface energy balances [top was with the BR approach, k_c as appropriate for each bridge (see section 3a), and $c_{pc} = 1380$ J kg^{-1} K^{-1}] and the NYSDOT thermocouple data, Q_I was estimated and compared with the calorimetry estimates (Fig. 16). Note that while the 1995, 1996, and 1999 calorimetry estimates were determined from the same batch of raw materials, the curves are slightly different. The differences arose because each sample contained a different amount of retarder, was started at a different temperature, or had a different amount of cement, all corresponding to the concrete when it was poured at each bridge (Table 1). These varied starting conditions resulted in different thermal conditions experienced by each sample in the calorimeter, and so the temperature-dependent heat evolution was also different.

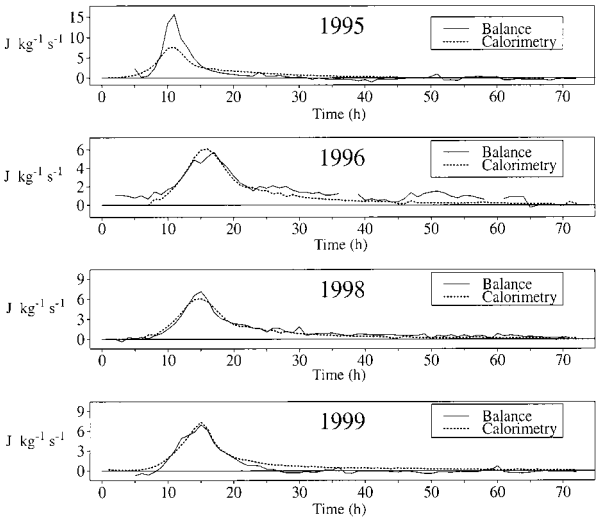

FIG. 16. Heat evolution rates estimated from the energy balances and calorimetry experiments for the four bridges. Note that the scale of the vertical axis for each bridge is different.

The calorimetry and energy balance estimates did not match exactly, since environmental conditions during curing for the samples were different. However, the energy balance and calorimetry estimates for the 1996, 1998, and 1999 bridges agree in terms of the peak heat evolution rate. For example, the 1999 energy balance heat evolution rate estimate peaked at about 6.9 joules per kilogram of cementitious solid per second, while the calorimetry estimate suggested a peak of about 7.3 J kg^{-1} s^{-1}. The peak rate for the 1996 bridge (6 J kg^{-1} s^{-1}) was lower than that for the 1998 or 1999 bridges because more retarder was used for the 1996 bridge and perhaps because of lower ambient air temperatures (Table 1).

For the 1995 bridge, 1) the concrete temperatures, when poured, were higher than the other bridges (Table 1), 2) no water was sprayed onto the bridge during stage 3, and 3) the concrete for this bridge (class H) had more cement than the others (class HP). These factors produced a much higher peak rate (15.6 J kg^{-1} s^{-1}) than the other bridges and shortened stage 3 as the hydration proceeded more quickly than at the other bridges. Because of heat loss from the calorimeter, the calorimetry sample hydrated more slowly and over a longer period than the 1995 concrete, producing a large disparity in calorimeter and energy balance heat evolution rates.

When integrated over the first 24 h after placement (which covers stages 2 and 3), the 1999, 1998, 1996, and 1995 energy balance estimates suggest, respectively, that about 173, 195, 200, and 275 kilojoules per kilogram of cementitious solid were liberated, in close

Unauthenticated | Downloaded 02/24/21 06:32 PM UTC

agreement with the calorimetry samples, which suggest, respectively, about 196, 195, 189, and 221 kJ kg^{-1} after 24 h. For the 1998 and 1999 bridges, which provided our most complete and reliable datasets, the 24-h energy balance estimates of the hydration heat source were within 12% of the calorimetry estimates. For the 1995 and 1996 bridges, for which many assumptions in determining the energy balances were made, the energy balance estimates were within about 20% of calorimetry estimates. This agreement of hydration heat estimates validates our methodology. Specifically, it validates the exchange coefficients calculated for the heat and moisture balances of these small areas both during periods when the concrete generated heat and later when the concrete was more passive in its environment.

The energy balance estimates of Q_I with the BR approach are dependent on the values chosen for k_c and c_{pc}. For the 1999 bridge, if $k_c = 2.4$ W m^{-1} K^{-1} and $c_{pc} = 1300$ J kg^{-1} K^{-1} (3 W m^{-1} K^{-1} and 1450 J kg^{-1} K^{-1}), reasonable values from our analysis, the energy balance estimate of 24-h heat generation would be 160 kJ kg^{-1} (187 kJ kg^{-1}) or 8% lower (higher) than the value with $k_c = 2.7$ W m^{-1} K^{-1} and $c_{pc} = 1380$ J kg^{-1} K^{-1}.

4. Conclusions and discussion

a. Findings

This work is the first to determine the complete energy balances of curing concrete bridge decks. The analysis of field, laboratory, and model data of four curing concrete bridge decks in eastern and central New York State has yielded the following important findings:

1) Between 70% and 85% of the heat transferred to or from the concrete occurred at the top surface. During the period of peak concrete temperatures at these bridges, sensible heat, latent heat, runoff water heat, and radiative fluxes, respectively, contributed 6%–24%, 15%–58%, 0%–73%, and 10%–34% of the top surface heat transfer.
2) Top surface latent and runoff water heat fluxes were most efficient at removing heat from the top surface, with the runoff flux dominating when winds were $<$ 1 m s^{-1}.
3) Because of insufficient fetch, direct eddy flux measurements were not as useful as flux-gradient techniques to estimate top surface latent and sensible heat fluxes. The largest uncertainty in determining vertical gradients of humidity and temperature was the burlap skin temperature which can vary by several degrees depending on location. Differences in air temperature and humidity measurements directly over the bridge and those from a tower several meters from the bridge were small and affected the estimated surface turbulent fluxes by $<$ 1%.
4) Computed exchange coefficients at a reference height of 0.9 m and with bulk Richardson number (Rb) > -0.2 averaged 0.0044, with a standard deviation of 0.0015. These coefficients are 1.5–2.5 times greater than those estimated with expressions for flow over a flat smooth plate, as used by Plawsky and Kapila (1997) for their predictions of bridge concrete temperatures and moisture. Our data suggest that for Rb < -0.2, exchange coefficients may be larger than 0.0044 if the surface-to-air virtual temperature differences ($T_{sv} - T_{av}$) are $<$ 5°C and smaller if $T_{sv} - T_{av} > 5$°C. Because of our limited dataset, the values for Rb < -0.2 must be used with caution.
5) More than 90% of the water sprayed onto the bridges ran off.
6) Water drops ejected from hoses on the bridge's top surface do not have sufficient fall distance to reach their equilibrium temperature which is within 0.5°C of the wet-bulb temperature of the air. Assuming they do reach their equilibrium temperature may result in errors of more than 25% in the runoff water heat flux.
7) Heat transfer at the bridge bottom was less than 30% of the top surface transfer and was dominated by conduction down the steel support beams.
8) Energy balance estimates of the 24-h total hydration heat of class-HP concrete from field data were within 20% of laboratory calorimetry estimates.
9) This project has supplied the first estimates of thermal conductivity (2.7–3.0 W m^{-1} K^{-1}), specific heat capacity ($\sim$1380 J kg^{-1} K^{-1}), density (2230 kg m^{-3}), and hydration heat (24-h heat $\sim$190 kJ kg^{-1}) of class-HP concrete.

b. Discussion

Because of the high costs of repairing or replacing concrete bridge decks, concrete bridges present a unique situation in which accurate estimates of surface fluxes over a small area (largest horizontal dimension $<$ 50 m) are of immediate practical importance. In the present work, common meteorological techniques to estimate energy balances, best suited for large patches or horizontally homogeneous areas, were shown to describe successfully the energy balances of an area as small as the bridges. The hydration heat from concrete's cementitious components provided the means with which to assess the quality of the energy balance estimates. The agreement of hydration heat estimates from laboratory calorimetry experiments and the field data validated our flux estimates and the exchange coefficients calculated for periods when the concrete generated heat and later when the concrete was more passive in its environment. These exchange coefficients, then, can be used to predict concrete bridge temperatures at any time.

Our directly measured eddy fluxes showed large disparities from those estimated with the flux-gradient techniques. This finding emphasizes the need to understand the influence of internal boundary layer development on the footprint of scalar concentrations, vertical scalar

Unauthenticated | Downloaded 02/24/21 06:32 PM UTC

profiles, and direct eddy flux measurements over small areas such as the bridge.

The energy balance estimates clearly show that to properly describe energy transfer to and from a curing concrete bridge deck, sensible heat, latent heat, runoff water heat, and radiative fluxes must be included. The magnitude of each flux varies depending on the ambient atmospheric and concrete conditions. Because current models do not contain these terms, the models cannot be accurately applied for a variety of atmospheric conditions.

The energy balance results from the present paper provide the boundary conditions for our model of curing concrete on bridge decks. A heat generation parameterization for class-HP concrete to be used in the model was developed from constant temperature calorimetry experiments in our laboratory (Wojcik et al. 2001, manuscript submitted to *Cem. Concr. Res.*). Once complete, the model will be used for sensitivity studies of the effect of atmospheric and concrete conditions on the thermal and moisture states of curing concrete. With these results, conditions under which a pour should not be allowed will be determined, information that potentially could save the NYSDOT millions of dollars in bridge repairs each year.

Future costs of concrete deck repairs due to cracking may also be reduced by mitigating heat loss through the beams, which produces thermal gradients and stresses within the concrete. Also, because excess water was sprayed onto the decks, construction project costs could be lowered by reducing the amount of spray water applied, especially in areas with limited water resources.

Although curing concrete bridges were the focus of this work, some of our methodology can be used successfully to estimate energy balances for any small areas (roads, fields, any concrete structure). For example, those concerned with estimating energy balances over fields irrigated with hoses or sprinklers may benefit from the finding that sprayed water drops may not spend enough time in the air to reach their equilibrium temperature, as Andreas (1990, 1995) has discussed.

Road condition prediction models can also benefit from our analysis. For example, in models to predict road temperature and ice occurrences, Sass (1992, 1997) and Jacobs and Raatz (1996) calculated exchange coefficients for convective fluxes with MOSH and assumed roughness lengths. Over surfaces the size of roads, it may be difficult to determine the proper roughness length. Our suggested exchange coefficients do not depend on the roughness length and can be determined with easily observed or predicted atmospheric and surface data.

During winter months, the beam heat transfer from a concrete deck no longer generating significant heat may cause ice to occur on the top surface above the beams before those areas above the form. Such information may be important to road surface temperature prediction models and road service personnel.

Acknowledgments. We gratefully acknowledge the partial funding support from the New York State Department of Transportation's Research and Development Bureau. From this office we acknowledge Dr. Robert Perry, Bob Valenti, Wes Yang, Rick Morgan, and Cheng Chou for their commitment to and assistance with the execution of the field work. We are indebted to the other members of the Jungle Research Group at the Atmospheric Sciences Research Center (ASRC) for their help in the field and in the laboratory: Dr. Kathleen Moore, Dr. Ricardo Sakai, Dr. Jeffrey Freedman, Dr. Otavio Acevedo, John Sicker, Dwayne Spiess, Behzad Abareshi, Ralf Staebler, and Matt Czikowsky. We thank Dr. Joel Plawsky of the Department of Chemical Engineering at Renssaeler Polytechnic Institute for his insight into the heat transfer of the bridges and Dr. Andrew Yencha of the University at Albany Chemistry Department for his help with the calorimetry. We also thank Mark Todaro of Benet Laboratories at the Watervliet Arsenal for producing the infrared images of the 1998 bridge. We are indebted to three anonymous reviewers whose comments and insights helped us to greatly improve this manuscript. Last, we extend our gratitude to the field engineers and construction personnel who provided us considerable freedom and assistance in setting up instruments and taking measurements.

APPENDIX

Definitions of Variables

$a0$	Intercept of the linear regression line from exchange coefficient/Rb data.
$a1$	Slope of the linear regression line from exchange coefficient/Rb data.
b	Coefficient for free convection exchange coefficient expression.
c_p	Moist air specific heat capacity (J kg^{-1} K^{-1}).
c_{pd}	Dry air specific heat capacity (J kg^{-1} K^{-1}).
c_{pc}	Concrete specific heat capacity (J kg^{-1} K^{-1}).
c_w	Water specific heat capacity (J kg^{-1} K^{-1}).
dT/dt	Time derivative of concrete temperatures (K s^{-1}).
dT/dz	Vertical linear concrete temperature gradient near the top surface (K m^{-1}).
g	Acceleration due to gravity (m s^{-2}).
k_c	Concrete thermal conductivity (W m^{-1} K^{-1}).
k_f	Thermal conductivity of the galvanized steel form (W m^{-1} K^{-1}).
k_s	Thermal conductivity of the steel beams (W m^{-1} K^{-1}).
nz	Total number of concrete layers: nine above the form and eleven above the beams.
q	Specific humidity measured with the krypton hygrometer on a boom (g g^{-1}).
q_a	Specific humidity of air measured with the Vaisala Humitter at 0.6 m (g g^{-1}).

Unauthenticated | Downloaded 02/24/21 06:32 PM UTC

q_a^* Saturation specific humidity at the air temperature (g g^{-1}).
q_s Specific humidity of air at the top surface assumed to be the saturation value at the top surface skin temperature T_s (g g^{-1}).
s Slope of the saturation specific humidity-versus-temperature curve (g g^{-1}).
$\overline{u'}$ East–west wind fluctuation (m s^{-1}).
$\overline{u'w'}$ Covariance of u' and w' (m^2 s^{-2}).
u_* Friction velocity (m s^{-1}).
$\overline{v'}$ North–south wind fluctuation (m s^{-1}).
$\overline{v'w'}$ Covariance of v' and w' (m^2 s^{-2}).
w Vertical wind speed (m s^{-1}).
$\overline{w'}$ Vertical wind fluctuations (m s^{-1}).
$\overline{w'q'}$ Covariance of the vertical wind and specific humidity fluctuations (m g g^{-1} s^{-1}).
$\overline{w'T_v'}$ Covariance of vertical wind and temperature fluctuations (m K s^{-1}).
$\overline{w'T'}$ Covariance of the vertical winds and virtual temperature fluctuations (m K s^{-1}).
z Distance above the surface (m).
z_0 Roughness length (m).
zc Concrete layer number.
A Surface area of the bridge (m^2).
C Exchange coefficient.
C_d Drag coefficient.
C_e Exchange coefficient for water vapor.
C_h Exchange coefficient for heat.
F_f Fraction of bottom area of the deck bounded by the form.
F_s Fraction of bottom area of the deck bounded by the beams.
G Proportionality constant.
L Obukhov length (m).
L_v Latent heat of vaporization of water (J kg^{-1}).
M Flow rate of water from the bridge (m^{-3} s^{-1}).
Q_H Surface sensible heat flux upwind of the bridge estimated with the footprint analysis (W m^{-2}).
Q_{HA} Sensible heat flux at the top surface of the bridge (W m^{-2}).
Q_E Surface latent heat flux upwind of the bridge estimated with the footprint analysis (W m^{-2}).
Q_{EA} Latent heat flux at the top surface of the bridge (W m^{-2}).
Q_{RA} Runoff water heat flux at the top surface of the bridge (W m^{-2}).
Q_{GA} Concrete heat flux at the top surface of the bridge (W m^{-2}).
Q_A^* Net radiation flux at the top surface of the bridge (W m^{-2}).
Q_{HB} Sensible heat flux at the bottom surface of the bridge (W m^{-2}).
Q_{GB} Concrete heat flux at the bottom surface of the bridge (W m^{-2}).
Q_B^* Net radiation flux at the bottom surface of the bridge (W m^{-2}).
Q_I Hydration heat source (W m^{-2}).
Rb Bulk Richardson number.
T' Air temperature fluctuations measured with the ATI sonic anemometer/thermometer (°C).
T Air temperatures measured with the ATI sonic anemometer/thermometer (°C).
$\overline{T}$ Mean air temperature over the period used to compute $\overline{w'q'}$ and $\overline{w'T'}$ (K).
T_a Air temperature measured by the Vaisala Humitter at 0.6 m (°C).
T_{av} Virtual temperature of air at 0.6 m (°C).
T_s Top surface skin temperature (°C).
T_{sv} Virtual air temperature at the surface (°C).
T_v Virtual temperature of air (°C).
T_{wf} Final spray-water temperature as it flowed off the bridge (°C).
T_{wi} Initial temperature of the spray water as it hit the top bridge surface (°C).
U Mean wind speed (m s^{-1}).
X Fetch over bridge up to the fast-response instruments (m).
α Priestley–Taylor parameter.
β Bowen ratio.
δ $s/(s + \gamma)$.
ε Emissivity of form or beams.
γ Psychrometric constant (c_p/L_v) (g g^{-1} K^{-1}).
ρ Air density (kg m^{-3}).
ρ_c Concrete density (kg m^{-3}).
ρ_w Density of water (kg m^{-3}).
σ_w Standard deviation of the vertical wind speed (m s^{-1}).
ΔQ_S Heat stored within the concrete deck (W m^{-2}).
ΔT_{cf} Temperature difference across 27-mm layer of concrete and steel in contact with the form (concrete temperature − form bottom temperature; °C).
ΔT_{cs} Temperature difference across 27-mm layer of concrete and steel in contact with the beams (concrete temperature − beam top temperature; °C).
$\Delta\overline{T}(zc)/\Delta t$ Time derivative of the mean concrete temperature at layer zc (°C m^{-1}).
Δz Approximate thickness of the top layer of concrete (m).
ΔZ_{cf} Thickness of concrete layer in contact with the form (27 mm).
ΔZ_{cs} Thickness of concrete layer in contact with the top of the beams (27 mm).
ΔZ_f Thickness of the form (4.8 mm).
ΔZ_s Thickness of layer of concrete in contact with the beam (32 mm).
$\Delta\overline{\Theta}_v$ Virtual potential temperature difference between the surface and the measurement height of 0.6 m (K).
$\overline{\Theta}_v$ Mean virtual potential temperature between the surface and the measurement height of 0.6 m (K).

Unauthenticated | Downloaded 02/24/21 06:32 PM UTC

REFERENCES

Alsayed, S. H., and M. A. Amjad, 1994: Effect of curing conditions on strength, porosity, absorptivity and shrinkage of concrete in hot and dry climate. *Cem. Concr. Res.,* **24,** 1390–1398.

Andreas, E. L, 1990: Time constants for the evolution of sea spray droplets. *Tellus,* **42B,** 481–497.

——, 1995: The temperature of evaporating sea drops. *J. Atmos. Sci.,* **52,** 852–862.

——, and B. A. Cash, 1999: Convective heat transfer over wintertime leads and polynyas. *J. Geophys. Res.,* **104,** 25 721–25 734.

Arya, S. P. S., 1977: Suggested revisions to certain boundary layer parameterization schemes used in atmospheric circulation models. *Mon. Wea. Rev.,* **105,** 215–227.

Brook, R. R., 1978: The influence of water vapor fluctuations on turbulent fluxes. *Bound.-Layer Meteor.,* **15,** 481–487.

Chiba, O., 1978: Stability dependence of the vertical wind skewness in the atmospheric surface layer. *J. Meteor. Soc. Japan,* **56,** 140–142.

de Bruin, H. A. R., and J. Q. Keijman, 1979: The Priestley–Taylor evaporation model applied to a large, shallow lake in the Netherlands. *J. Appl. Meteor.,* **18,** 898–903.

Dyer, A. J., and T. V. Crawford, 1965: Observations of the modification of the microclimate at a leading edge. *Quart. J. Roy. Meteor. Soc.,* **91,** 345–348.

FitzGibbon, M. E., 1976a: Large pours for reinforced concrete structures. *Concrete,* **10** (3), 41.

——, 1976b: Large pours—2, heat generation and control. *Concrete,* **10** (12), 33–35.

Garratt, J. R., 1992: *The Atmospheric Boundary Layer.* Cambridge University Press, 316 pp.

Geiger, R., 1965: *The Climate Near the Ground.* Harvard University Press, 611 pp.

Gopalan, M. K., and M. N. Haque, 1987: Effect of curing regime on the properties of fly-ash concrete. *Amer. Concr. Inst. Mater. J.,* **84** (1), 14–19.

Horst, T. W., 1997: The footprint for estimation of atmosphere–surface exchange fluxes by eddy-correlation and profile techniques. Preprints, *Special Symp. on Boundary Layers and Turbulence,* Long Beach, CA, Amer. Meteor. Soc., 58–64.

——, and J. C. Weil, 1994: How far is far enough? The fetch requirements for micrometeorological measurement of surface fluxes. *J. Atmos. Oceanic Technol.,* **11,** 1018–1025.

Hughes, B. P., and A. T. Mahmood, 1988: Laboratory investigation of early thermal cracking of concrete. *Amer. Concr. Inst. Mater. J.,* **85** (3), 164–171.

Idso, S. B., 1981: A set of equations for full spectrum and 8- to 14-μm and 0.5- to 12.5-μm thermal radiation from cloudless skies. *Water Resour. Res.,* **17,** 295–304.

Itier, B., Y. Brunet, K. J. McAneney, and J. P. Lagouarde, 1994: Downwind evolution of scalar fluxes and surface resistance under conditions of local advection. *Agric. For. Meteor.,* **71,** 211–225.

Jacobs, W., and W. E. Raatz, 1996: Forecasting road-surface temperatures for different site characteristics. *Meteor. Appl.,* **3,** 243–256.

Kaimal, J. C., and J. J. Finnigan, 1994: *Atmospheric Boundary Layer Flows.* Oxford University Press, 289 pp.

——, J. C. Wyngaard, Y. Izumi, and O. R. Coté, 1972: Spectral characteristics of surface-layer turbulence. *Quart. J. Roy. Meteor. Soc.,* **98,** 563–589.

Kapila, D., J. Falkowsky, and J. L. Plawsky, 1997: Thermal effects during the curing of concrete pavements. *Amer. Concr. Inst. Mater. J.,* **94** (2), 119–128.

Kinzer, G. D., and R. Gunn, 1951: The evaporation, temperature, and thermal relaxation-time of freely falling waterdrops. *J. Meteor.,* **8,** 71–83.

Kondo, J., and S. Ishida, 1997: Sensible heat flux from the earth's surface under natural convection conditions. *J. Atmos. Sci.,* **54,** 498–509.

Kristensen, L., and D. R. Fitzjarrald, 1984: The effect of line averaging on scalar flux measurements with a sonic anemometer near the surface. *J. Atmos. Oceanic Technol.,* **1,** 138–146.

——, J. Mann, S. P. Oncley, and J. C. Wyngaard, 1997: How close is close enough when measuring scalar fluxes with displaced sensors? *J. Atmos. Oceanic Technol.,* **14,** 814–821.

Lachemi, M., and P.-C. Aïtcïn, 1997: Influence of ambient and fresh concrete temperatures on the maximum temperature and thermal gradient in a high performance concrete structure. *Amer. Concr. Inst. Mater. J.,* **94** (2), 102–110.

Laubach, J., and K. G. McNaughton, 1998: A spectrum-independent procedure for correcting eddy fluxes measured with separated sensors. *Bound.-Layer Meteor.,* **89,** 445–468.

Monteith, J. L., 1965: Evaporation and environment. *Symp. Soc. Exp. Biol.,* **19,** 205–234.

Neville, A. M., 1996: *Properties of Concrete.* John Wiley and Sons, 844 pp.

NYSDOT, 1995: The ''state of the art'' bridge deck. Bridge Deck Task Force Rep., 58 pp. [Available from New York State Department of Transportation Structures Division, 1220 Washington Ave., Building 5, 6th Floor, W. Averell Harriman State Office Building Campus, Albany, NY, 12232-0600.]

——, 1999: Specification revisions-class HP concrete for substructures and structural slabs. NYSDOT Rep. EI 99-002, 22 pp. [Available from New York State Department of Transportation Structures Division, 1220 Washington Ave., Building 5, 6th Floor, W. Averell Harriman State Office Building Campus, Albany, NY, 12232-0600.]

Oke, T. R., 1987: *Boundary Layer Climates.* Methuen and Co., 435 pp.

Panofsky, H. A., and J. A. Dutton, 1984: *Atmospheric Turbulence: Models and Methods for Engineering Applications.* Wiley and Sons, 397 pp.

Penman, H. L., 1948: Natural evaporation from open water, bare soil, and grass. *Proc. Roy. Soc. London,* **A193,** 120–195.

Philip, J. R., 1961: The theory of heat flux meters. *J. Geophys. Res.,* **66,** 571–579.

Plawsky, J. L., and D. Kapila, 1997: Cement hydration and heat exchange for curing process of bridge decks at early stages. NYSDOT Rep., 24 pp. [Available from New York State Department of Transportation Research and Development Bureau, 1220 Washington Ave., Building 7A, 7th Floor, W. Averell Harriman State Office Building Campus, Albany, NY, 12232-0600.]

Prata, A. J., 1996: A new long-wave formula for estimating downward clear-sky radiation at the surface. *Quart. J. Roy. Meteor. Soc.,* **122,** 1127–1151.

Priestley, C. H. B., and R. J. Taylor, 1972: On the assessment of surface heat flux and evaporation using large-scale parameters. *Mon. Wea. Rev.,* **100,** 81–92.

Pruppacher, H. R., and J. D. Klett, 1997: *Microphysics of Clouds and Precipitation.* Kluwer Academic, 954 pp.

Rao, K. S., 1975: Effect of thermal stratification on the growth of the internal boundary layer. *Bound.-Layer Meteor.,* **8,** 227–234.

Rogers, R. R., and M. K. Yau, 1989: *A Short Course in Cloud Physics.* Pergamon Press, 293 pp.

Sass, B. H., 1992: A numerical model for prediction of road temperature and ice. *J. Appl. Meteor.,* **31,** 1499–1506.

——, 1997: A numerical forecasting system for the prediction of slippery roads. *J. Appl. Meteor.,* **36,** 801–817.

Scanlon, J. M., and J. E. McDonald, 1994: Thermal properties. *Significance of Tests and Properties of Concrete and Concrete-Making Materials,* P. Klieger and J. Lammond, Eds., American Society for Testing and Materials, 229–239.

Schmid, H. P., 1997: Experimental design for flux measurements: Matching scales of observations and fluxes. *Agric. For. Meteor.,* **87,** 179–200.

Stannard, D. I., 1997: A theoretically based determination of Bowen-ratio fetch requirements. *Bound.-Layer Meteor.,* **83,** 375–406.

Stewart, R. B., and W. R. Rouse, 1977: Substantiation of the Priestley

Unauthenticated | Downloaded 02/24/21 06:32 PM UTC

and Taylor parameter $\alpha = 1.26$ for potential evaporation in high latitudes. *J. Appl. Meteor.*, **16,** 649–650.

Stull, R. B., 1988: *An Introduction to Boundary Layer Meteorology.* Kluwer Academic, 666 pp.

Tan, K., and O. E. Gjorv, 1996: Performance of concrete under different curing conditions. *Cem. Concr. Res.*, **26** (3), 355–361.

Ulm, F.-J., O. Coussy, and C. Hellmich, 1998: Chemoplasticity: A review of evidence. *Computational Modeling of Concrete Structures,* R. de Borst et al., Eds., A and A Balkema, 421–439.

Walmsley, J. L., 1989: Internal boundary layer height formulae—a comparison with atmospheric data. *Bound.-Layer Meteor.*, **47,** 251–262.

Wojcik, G. S., 2001: The interaction between the atmosphere and curing concrete on bridge decks. Ph.D. dissertation, University at Albany, State University of New York, 175 pp.

Wyngaard, J. C., O. R. Coté, and Y. Izumi, 1971: Local free convection, similarity, and the budgets of shear stress and heat flux. *J. Atmos. Sci.*, **28,** 1171–1182.

Unauthenticated | Downloaded 02/24/21 06:32 PM UTC